# DEVELOPMENT OF THE IBR PULSED REACTOR AND ITS USE IN SCIENTIFIC RESEARCH

I. M. Frank

The IBR factors are described, and their basic characteristics are given. There is a brief outline of the basic studies which have been carried out in the Neutron Physics Laboratory of the Joint Institute for Nuclear Research since the reactors have been available.

## 1. Stages in the Development of the Neutron Physics Laboratory

Since June 23, 1960, when the IBR reactor first achieved pulsed criticality [1, 2], this reactor has governed the basic scientific directions in the Neutron Physics Laboratory (NPL) of the Joint Institute for Nuclear Research (JINR). Since a decade is a long time, we should look back to see how fruitful the use of the pulsed reactor and its injector modification has been, to determine the basic results which have been achieved, and to analyze the outlook for the future. Although this review is not a jubilee or memorial review, like any review it contains results and illustrations from various years, including some from a decade ago.

We start with a brief review of the history of the IBR reactor and its development. Planning of the IBR reactor seems to have been begun in the Physicoenergetics Institute in 1955, on the initiative of D. I. Blokhintsev. The Joint Institute for Nuclear Research entered the picture in 1957, and construction and preparation for the experiments were begun. The IBR reactor was constructed, started up, and first used jointly by the Neutron Physics Laboratory and the Physicoenergetic Institute.

Figure 1 shows the layout of the IBR reactor, taken from the first laboratory report of the Scientific Council of the JINR after the start-up [2]; the layout has not been changed radically since. Two bushings 2 are mounted in steel disc 1. One bushing was originally made of $^{235}U$ and the other, acting as a counterweight, of $^{238}U$; at present, both bushings are of $^{235}U$. Both weight about 4 kg and are carefully machined to be nearly identical. On both sides of the disc are two casettes containing air-cooled plutonium rods 4. About 20 kg of plutonium is used. Electric motor 13 drives the primary disc at 3000 rpm through gear system 11. The same apparatus is used to transmit the rotation to an auxiliary disc, which also contains a uranium bushing. The number of revolutions which the auxiliary disc undergoes for each revolution of the primary disc can be adjusted, so the repetition frequency of the reactor pulses can be adjusted.

Figure 2 shows the reactor and reactor room as they would appear if part of the biological-shielding wall were removed and if the experimental apparatus were removed. To the left of the reactor is a carriage, at one end of which there is lead shielding which shields the active zone when the reactor is shut down. At the other end of the carriage are cassettes containing a hydrogenous material which is used to produce thermal and resonance neutrons. They are moved into the active zone before the start-up.

Figure 2a shows the members of the FTI and JINR who participated in the reactor start-up after construction; Fig. 2b shows the control panel. These figures date from 1960.

Joint Institute for Nuclear Research, Dubna. Translated from Problemy Fiziki Élementarnykh Chastits i Atomnogo Yadra, Vol. 2, No. 4, pp. 805-860, 1972.

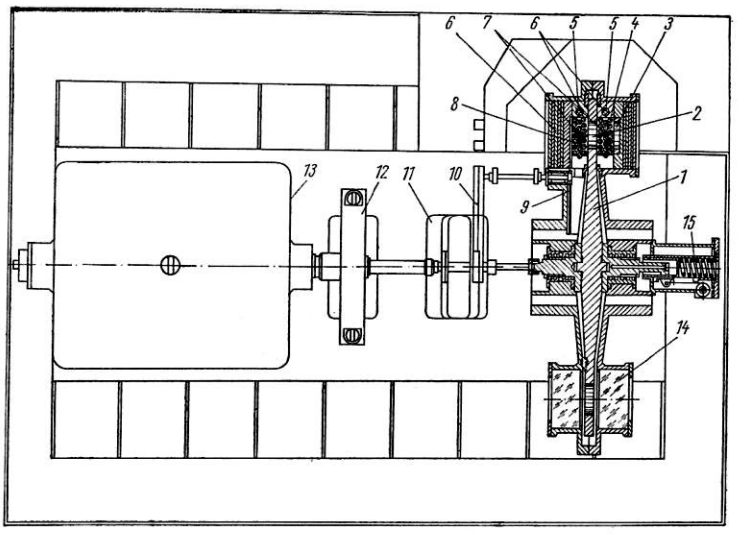


Fig. 1. The IBR reactor. 1) Primary rotating disc; 2) primary movable zone; 3) coarse-regulator plate; 4) fixed active zone; 5) automatic and manual control rods; 6) neutron reflector; 7) emergency rods; 8) auxiliary movable zone; 9) auxiliary rotating disc; 10) linkage to the shaft of the auxiliary disc; 11) gear system for increasing the number of revolutions; 12) brake for rapidly stopping the rotation; 13) electric motor for rotating the disc; 14) control system for covering the primary movable zone; 15) mechanism for slow rotation of the disc.

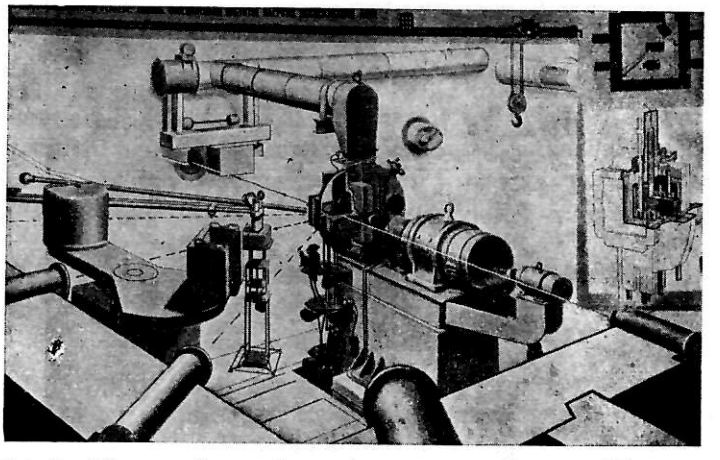

Fig. 2. The reactor and reactor room as they would appear if part of the biological-shielding wall were removed and certain parts of the reactor were cut away. The broken lines represent neutron ducts passing through the center of the active zone. Shown in larger scale at the right is the active zone.

The IBR reactor was designed for operation at an average power of 1 kW, and this consideration largely governed its construction. By the end of 1960 it had reached its planned power, and physical experiments involving the neutron beams were begun. A power of 3 kW turned out to be the optimum power for the reactor design (but not for the physicists, who were always interested in an increased neutron flux),

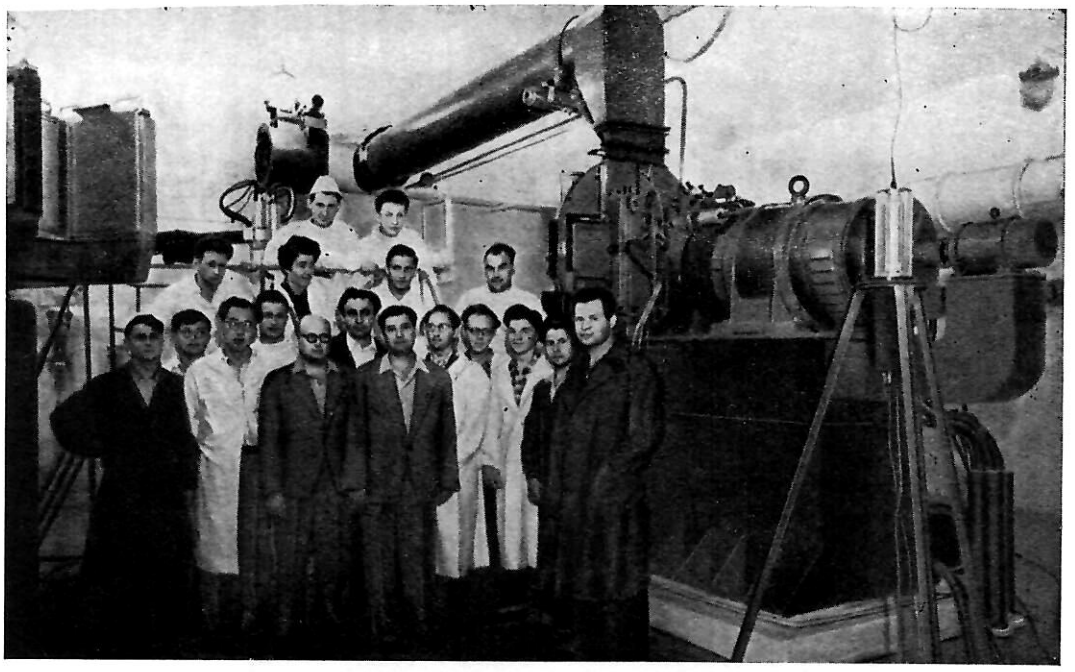

Fig. 2a. Participants in the start-up of the IBR reactor in June, 1960

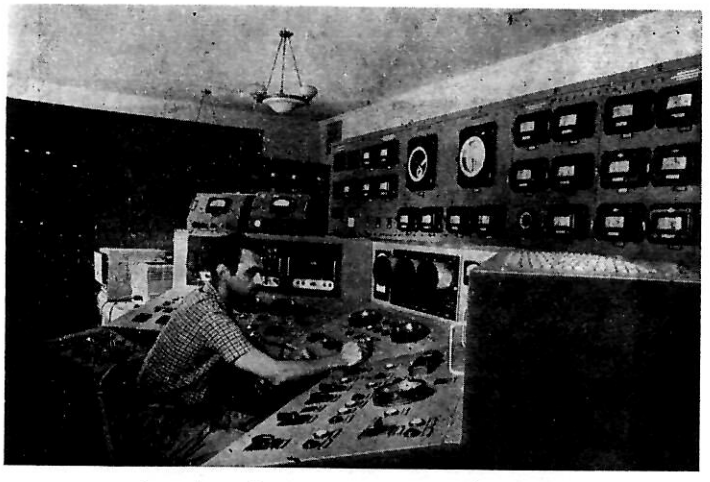

Fig. 2b. The reactor control panel.

so this power was used in most of the experiments. The reactor was usually operated at 5 pulses/sec, and the instantaneous power per pulse was about 15 MW. The length of a reactor pulse was (not unexpectedly) about 50 $\mu$sec. Over a 1000-m baseline, this length resulted in a resolution of 0.05 $\mu$sec/m. This was a good resolution at that time, but not the best which had been achieved in a time-of-flight spectrometer. In view of the rapid progress which was being made in the resolution of neutron spectrometers, this circumstance caused some anxiety from the very beginning and stimulated a search for methods to improve the resolution. Ultimately, this search resulted in the construction of an electron accelerator which was used as a neutron injector. Originally, this accelerator was a 30-MeV microtron. A uranium target in the active zone of the reactor was bombarded by electrons, and photoneutrons were produced in it. The reactor operated in the subcritical mode for this purpose, with a booster which multiplied the neutron burst by a factor of 100 or 200. A microtron was chosen as injector because it could be placed in a room available above the reactor room and because it could be constructed relatively quickly. This work was carried out by the NPL and the Institute of Physical Problems, Academy of Sciences of the USSR (in the

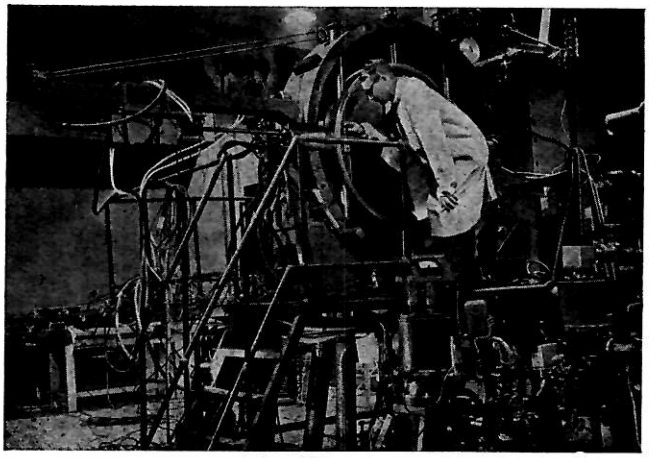

Fig. 3. The microtron which was used from 1964 to 1968 as an injector for the IBR reactor.

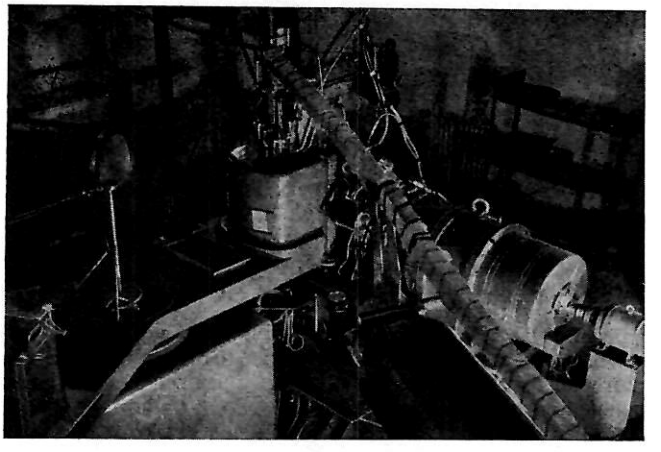

Fig. 4. The IBR reactor in 1968.

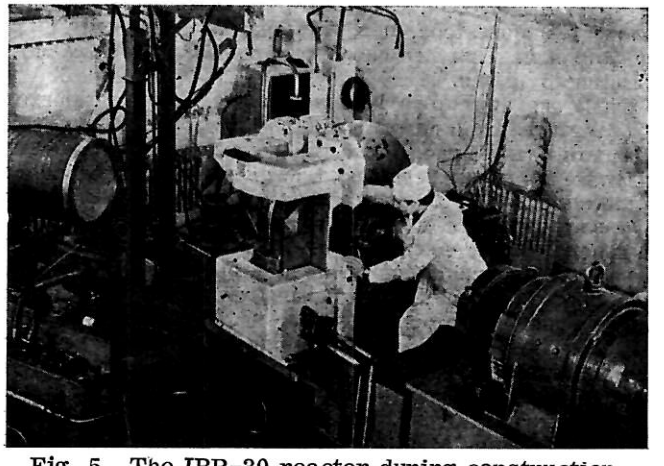

Fig. 5. The IBR-30 reactor during construction.

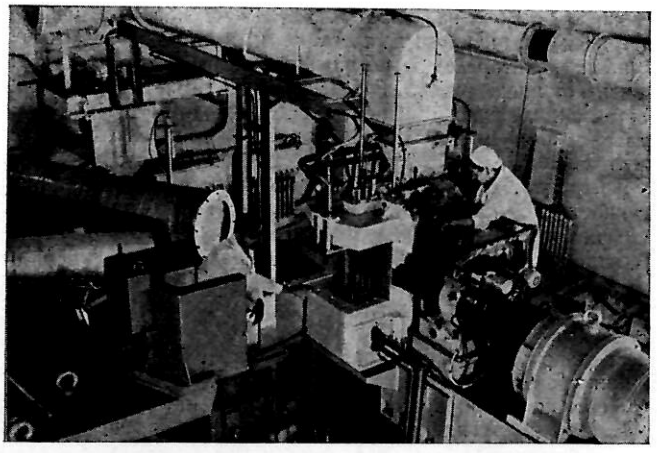

Fig. 6. The IBR-30 reactor before the 1969 start-up.

laboratory of S. P. Kapitsa); the injector was put into operation in 1964 [3]. Figure 3 shows the microtron. The length of the reactor pulse was decreased by more than an order of magnitude through the use of this injector. At 50 pulses/sec having a length of 3-4 $\mu$sec, the average reactor power was about 0.5 kW, i.e., about one-sixth that without the injector.

In the summer of 1968 the IBR reactor was first used in the isolated-pulse mode (one pulse per several seconds). The average power was 6 kW, while the instantaneous power reached a million kilowatts. Figure 4 shows the reactor in 1968; here the reactor room is filled with neutron ducts and apparatus for producing the neutron beams, as can be seen clearly by a comparison with Fig. 2a. When a new and refined reactor was constructed in 1968, the IBR reactor was shut down, in August, and the reactor and microtron were disassembled. The new reactor, the IBR-30, was installed in the place of the former reactor and was started up on June 10, 1969 [4]. Figure 5 shows the IBR-30 during its construction. The steel disc is being adjusted, and the uranium bushings have not yet been put in place. Cassettes for the plutonium rods are mounted within the massive base, which is shaped like the letter "П" lying on its side.

Figure 6 shows the IBR-30 after the construction. At the left of the electric motor is a complicated gear box which is used for remote adjustment of the rotation rate of the disc with the auxiliary active zone. The IBR-30 reactor now has an average power of 25 kW, i.e., eight times that of its predecessor.

A new injector was put into operation on March 24, 1970: a 30-MeV linear electron accelerator. The electrons bombard a plutonium carbide target; at 100 pulses/sec and a multiplication factor of 100, for which the pulse length is about 3 $\mu$sec, the reactor power is about 3 kW. Accordingly, like the power of the first reactor without the injector, this power is six times that of the reactor with the microtron injector. With a 1000-m baseline, the resolution is 3 nsec/m.

Figure 7 shows the injector, whose accelerating tube is vertical, on top of the reactor. Figure 8 shows the outside of the reactor building. The linear accelerator is installed in the enclosure on the roof. Below it is the new experimental room, constructed in 1969 along with the IBR-30. Finally, Fig. 9 shows the housing of the 1000-m neutron duct as viewed from the top of the reactor building. The three-story building which the housing passes through holds the reactor control panel. Beyond this building is one housing the laboratories of the NPL; the tower houses a 4.5-MeV electrostatic accelerator.

In the review below of the various experiments which have been carried out, we will not discuss the experimental methods in detail. We simply show, in Figs. 10 and 11, a general view of the Central Measurement Center of the NPL, which receives information from all the measurement apparatus in the eight operating channels of the reactor. These channels range in length from 1000 to 10 m. The analyzers in the measurement center store and sort the information, which can then be transmitted for analysis to a BÉSM-4 computer, in a room adjacent to the Measurement Center, separated from it by a glass wall.

The IBR reactor operates by a unique mechanism different from that of ordinary stationary reactors and from that of pulsed reactors in which each pulse is independent of the preceding pulses. In the IBR reactor, the radiation pulse is triggered by delayed neutrons produced in preceding pulses; the pulse must

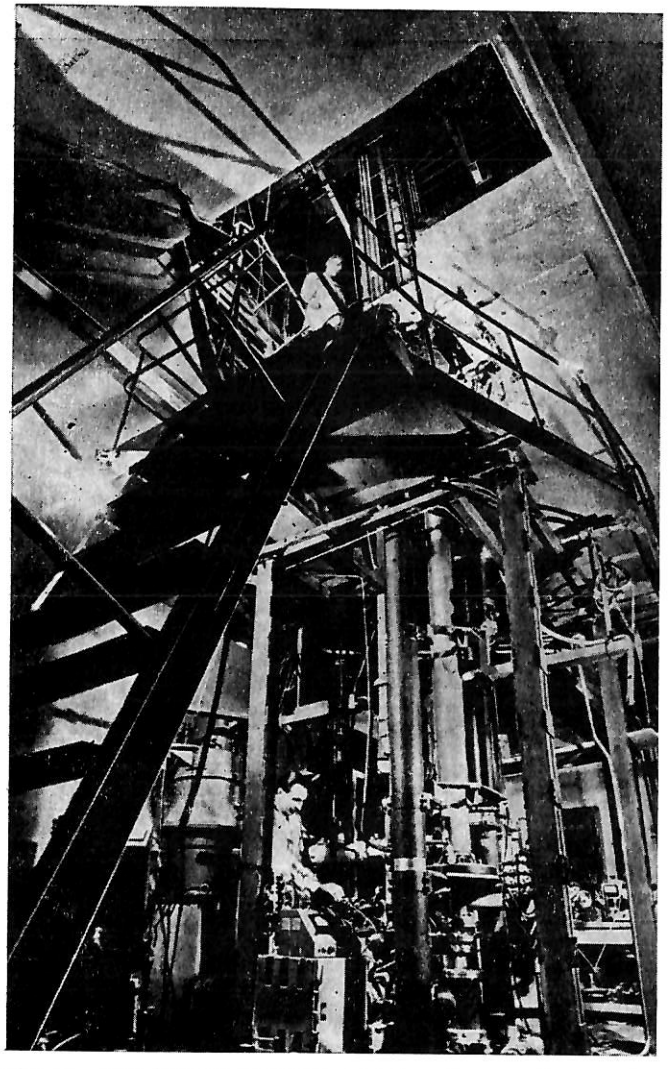

Fig. 7. The linear electron accelerator used as an injector for the IBR-30 reactor.

Fig. 8. The reactor building.

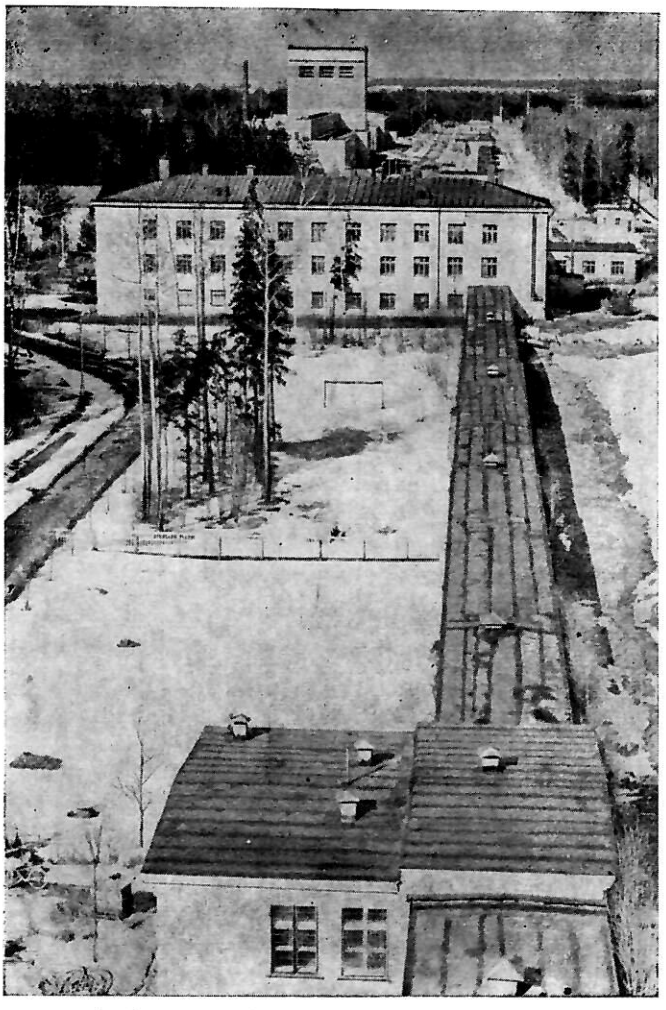

Fig. 9. The housing of the 1000-m neutron duct as viewed from the top of the reactor building.

Fig. 10. Measurement center of the NPL.

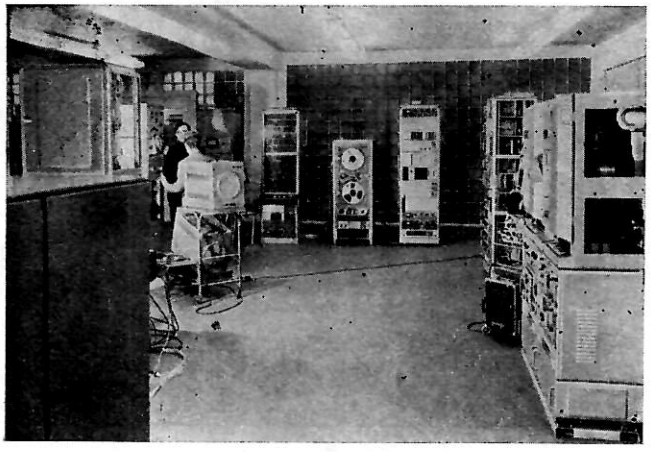

Fig. 11. Measurement center of the NPL. A BÉSM-4 computer is installed behind the glass wall.

include enough fission events to make up for the loss of delayed neutrons by the radiators. This type of operation requires a very definite subcriticality (the "pulsed criticality") in terms of prompt neutrons.

The theory of the IBR reactor was first worked out by Bondarenko and Stavisskii [5]. The basic equations are shown in Appendix 1; here we merely note that they have been well supported by experiment.

We can briefly summarize the parameters of the IBR-30 reactor: it can operate at an average power of 25 kW at 100 and 4 pulses/sec (the first mode is the usual one when the injector is used). It is also possible to operate at other pulse repetition frequencies, and even in the isolated-pulse mode (1 pulse per 4.7 sec or per 7.6 sec). The instantaneous power in the isolated-pulse mode does not exceed $10^6$ kW.

In the ordinary mode of 4 pulses/sec at an average power of 25 kW, a total of $1.2 \cdot 10^{15}$ neutrons/sec are emitted into a solid angle of $4\pi$, and the instantaneous power reaches 100 MW, a typical figure for reactors having a high flux density.

In many problems an important consideration is the thermal-neutron flux from 1 $cm^2$ of moderator. At 25 kW this flux has an average value of $\bar{n}_{ther} = 5 \cdot 10^{10}$ neutrons/($cm^2 \cdot$ sec). The average neutron flux thus is not high. At 4 pulses/sec, the neutron flux curve pulse is about $n_{ther} = 10^{14}$ neutrons/$cm^2$ (the thermal-neutron flux within the moderator is an order of magnitude higher, i.e., about $10^{15}$ neutrons/$cm^2$). Since the entire moderator area, $\sim 10^3$ $cm^2$, can be used in time-of-flight experiments, the IBR reactor is extremely efficient for such experiments. Appendix 2 gives some information about the history of the reactor, along with data on the pulse length, etc.

Historically, there has been a prolonged competition between accelerators and reactors in the development of neutron optics and spectroscopy. The advantages of reactors in the thermal-neutron and cold-neutron ranges are now quite obvious, as are the advantages of pulsed accelerators in the resonance-neutron range, because of their high resolution.

The IBR reactor was planned for relatively few types of experiments. Over the years, however, the experiments have become more and more varied, apparently for at least two objective reasons: First, the constantly increasing emphasis on neutron-physics experiments requires the use of spectroscopic methods; second, the IBR reactors with and without the injector combine advantages of both reactors and accelerators for such experiments.

The only spectroscopic experiments which cannot be carried out with the injector-equipped IBR are those which require an extremely high resolution over a wide range of neutron energies. Such experiments may become crucial in the future, e.g., for studying the shape of a large number of resonances. However, the present trend in neutron physics is toward experiments requiring higher and higher beam intensities at an adequate energy resolution.

Existing high-flux steady-state reactors provide thermal-neutron fluxes on the order of $\bar{n}_{ther} = 10^{15}$ neutrons/($cm^2 \cdot$ sec) at a power of 50-100 MW. This power level is evidently near the practical limit for a steady-state reactor.

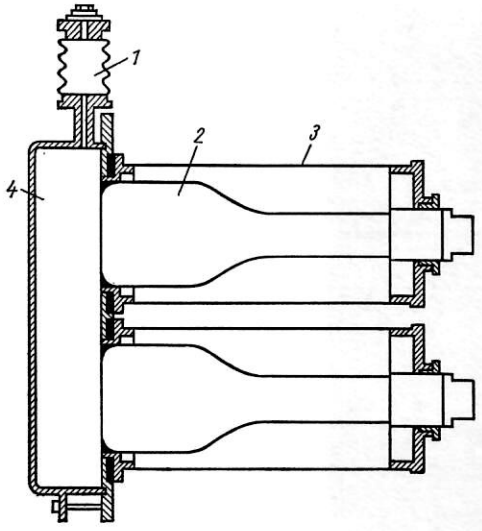


Fig. 12. The scintillation neutron detector used to measure transmission curves. 1) Bellows; 2) photomultiplier; 3) housing; 4) scintillator.

The IBR-30 produces pulsed thermal-neutron flux densities on the same order of magnitude at an average power of only 25 kW. Even this power, however, is not far from the practical limit, probably on the order of 100 kW for an air-cooled reactor of the IBR type. This power limit can be significantly raised by converting to liquid-metal cooling. The pulsed-neutron flux could be raised by at least two orders of magnitude, i.e., to about $n_{ther} = 10^{17}$. The construction of such a reactor, the IBR-2, having an average power of 4 MW, was begun at the JINR in 1969 [6]. Hopefully, this reactor will be started up within the next 4 yr. Not only does this reactor extend the range of previous experiments: it also makes several new experiments possible. An electron-accelerator injector of a relatively high power is planned for this reactor.

## 2. Development of Physical Research Using Resonance Neutrons

Below we will briefly review the various directions of this research, especially those for which the use of the IBR reactor with and without the injector has proved fruitful. Obviously, we cannot review each study, since there have been many of them over the past decade.

We can classify the studies into three groups: neutron spectroscopy of nuclei; study of the properties of the neutron, i.e., elementary-particle physics; and study of condensed media. In several cases, however, these groups overlap so much that it is difficult to distinguish among them. Here we will not attempt to follow this classification; we will discuss research involving resonance and thermal neutrons.

A. Neutron Spectroscopy of Nonfissionable Nuclei. The scientific interests of the group which began working at the NPL at the time of the reactor start-up led naturally to neutron spectroscopy of nuclei, and these studies are still being carried out. From the very beginning there has been interest in the properties of the individual resonances. Even before the start-up, Yazvitskii et al. [7] built a liquid-scintillator detector for measuring transmission curves [8] (Figs. 12 and 13), and Pikel'ner et al. [9] constructed a two-section cylindrical liquid detector for detecting capture $\gamma$ rays (consisting of about 450 liters of toluene with scintillating admixtures). The test sample is placed in the hollow inner part of the detector, through which a well-collimated neutron beam passes (Figs. 14 and 15; these illustrations are taken from a 1960 report; i.e., they are as old as the reactor). These detectors are still in use today, although with some modifications. The radiative-capture detector, e.g., is sectioned in a different manner, and methyl borate has been added to it to reduce the hard-$\gamma$ background due to neutrons scattered by the sample and absorbed in the detectors.

Somewhat later, in 1964, a liquid detector was constructed for studying fissionable materials (Fig. 16); with it, samples weighing up to 200 g-wt can be studied. This detector distinguishes fission from radiative capture, since the fission neutrons, slowed in the detector and absorbed in the cadmium propionate in it, produce delayed coincidences.

In reviewing the development of neutron-spectroscopy research, we must not forget that in 1960 the experimental base for the development of theory regarding the neutron resonances was far from solid. The optical-model predictions regarding the force function were based on data for only a few resonances, generally obtained by averaging data over resonances differing in spin. Information was available for relatively few nuclei, and primarily for mixtures of isotopes. No systematic data were available for the radiation widths, and spectroscopy of fissionable elements was limited to the low-energy range. The detectors available could determine the total and partial widths of the resonances $\Gamma$, $\Gamma_\gamma$, $\Gamma_f$, $g\Gamma_n$; in certain cases they could determine the statistical factor $g = (2J + 1)/2(2I + 1)$, and thus the spin J of the resonance ($J = I \pm 1/2$, where I is the spin of the target nucleus). These detectors thus resolved certain ambiguities, and a systematic study of the resonances was begun.

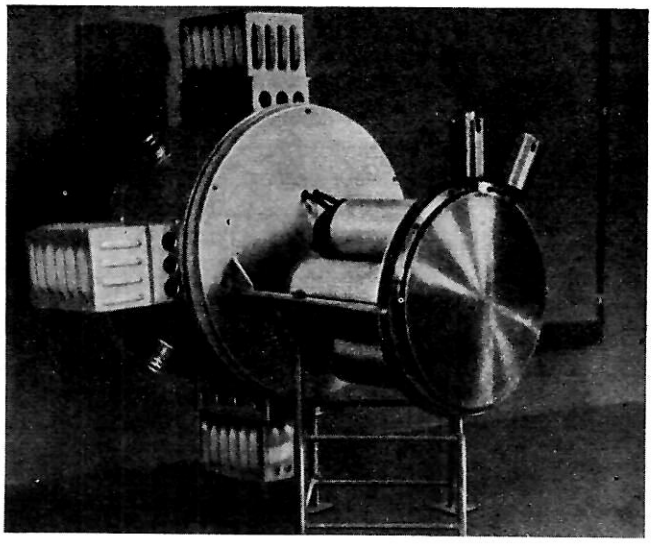

Fig. 13. The scintillation neutron detector.

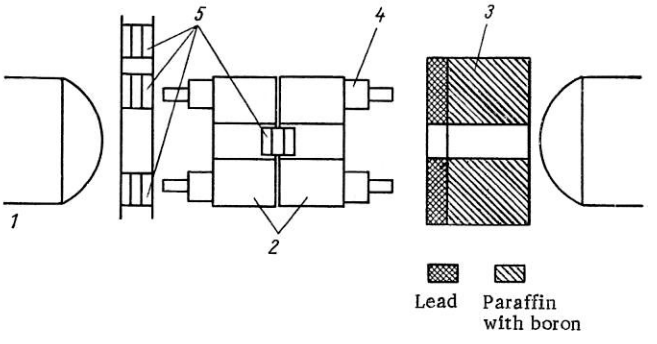


Fig. 14. Apparatus used to measure the cross section for radiative neutron capture. 1) Neutron duct; 2) scintillators; 3) collimators; 4) photomultiplier; 5) samples.

About 30 elements have been studied in the NPL; during the last 5 yr, the study has been extended to individual isotopes, including those of some of the multiisotope rare earths. About 60 isotopes have been studied.

The statistical method in nuclear theory led to a unique and essentially paradoxical approach to the analysis of the neutron-spectroscopy results, and to a large extent, this is still the situation today. Spectroscopy is used to study the individual parameters of the resonances – not in order to reach conclusions about the nature of the resonances, but in order to establish statistical regularities on the basis of data for many resonances. According to this approach, success depends largely upon the volume of information obtained; this volume has in fact been large and has furnished an adequate basis for several conclusions. Here, of course, we can discuss only some of the results.

The most definite results concern the total radiation widths $\Gamma_\gamma$, whose values fluctuate so little from level to level that conclusions can be reached on the basis of a relatively few resonances for a given nucleus. The experimental procedure and the interpretation of the results are not very simple, as can be seen from the following example. In a comparatively recent study, published in 1968, Glass et al. [11] concluded that the radiation width $\Gamma_\gamma$ for the $^{238}U$ resonances was different from that reported previously in [12, 13] and – most significantly – that the $\Gamma_\gamma$ values went through approximately two periodic fluctuations as functions of the neutron energy below 2 keV. Reports of periodic changes in neutron parameters, sometimes not justified, are currently fashionable. On the other hand, some fissionable elements do in fact

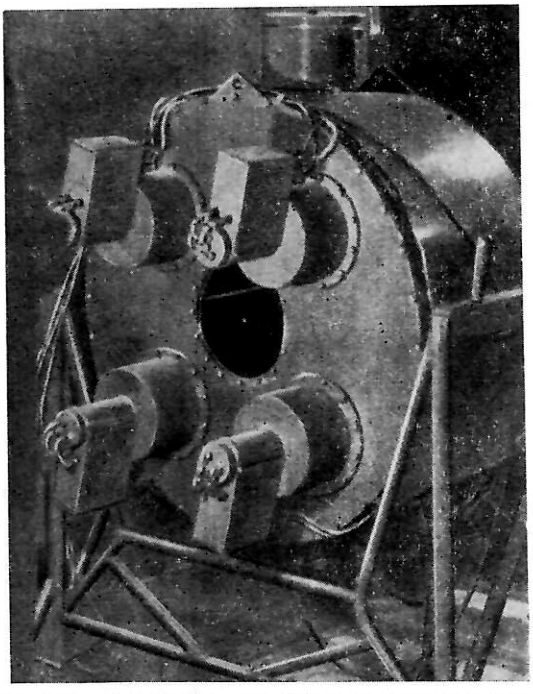

Fig. 15. The liquid-scintillator detector for detecting radiative neutron capture.

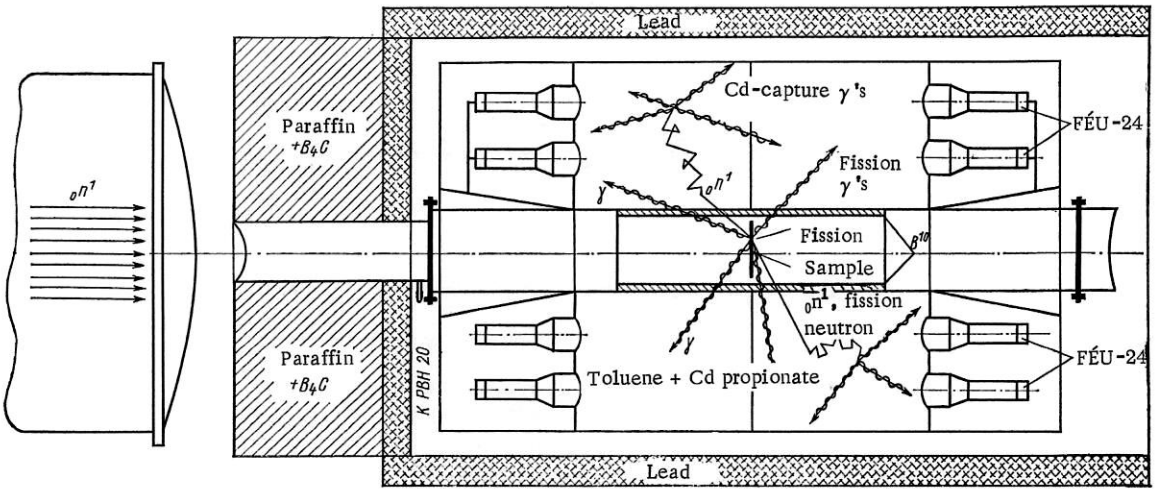


Fig. 16. The liquid-scintillator detector for studying fissionable materials.

display fluctuations in, at least, the fission cross section, so this result received serious attention. Careful studies by Soviet scientists [14], based on $\Gamma_\gamma$ measurements for thirty resonances below 1.5 keV, showed that the radiation width remained constant within a few percent. We can apparently conclude that measurements with a periodic pulsed neutron source, such as the injector-equipped IBR reactor, have advantages in at least some cases over measurements based on the single pulse from a nuclear explosion, such as those in which Glass et al. reached their conclusion (although the resolution in their experiments are considerably better).

Figure 17, from [15], compares all the available data on radiation widths. In addition to the systematic A dependence of $\Gamma_\gamma$, we see that there are also fluctuations from nucleus to nucleus which are not experimental errors (the scatter in the calculated points shows that a smooth curve cannot be expected).

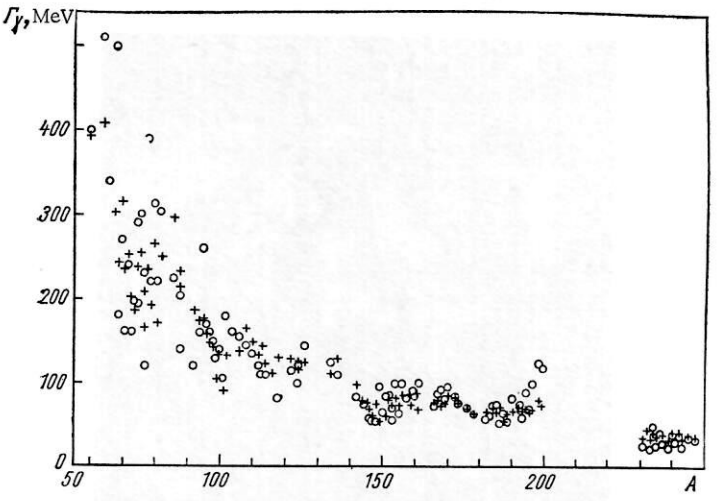


Fig. 17. Experimental (circles) and calculated (plus signs) values of $\Gamma_\gamma$.

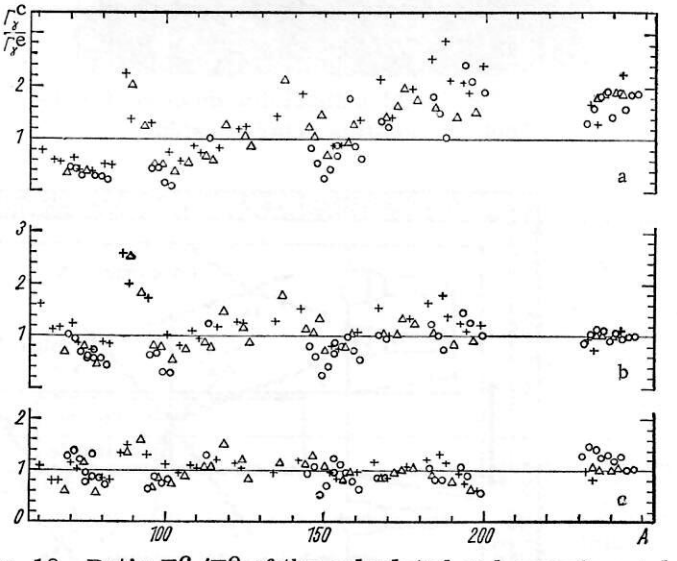


Fig. 18. Ratio $\Gamma_\gamma^c/\Gamma_\gamma^e$ of the calculated and experimental radiation widths: a) $\Gamma_\gamma^c = 81 \cdot 10^{-6} A^{7/3} U^{2.2} a^{-2.8}$; b) $\Gamma_\gamma^c = 0.10 A^{2/3} U^{1/8} a^{-2.2}$; c) $\Gamma_\gamma^c = 8.7 A^{-0.9} U^{-0.9} a^{-0.57}$.

Theoretical predictions can be found by approximating the theoretical expressions found by Weisskopf and Axel on the basis of the statistical model. Figure 18 compares theory and experiment. The calculated value $\Gamma_\gamma$ can be represented as the product of three quantities, raised to powers x, y, and z, respectively: the mass number $A^x$, the effective excitation energy $U^y$, and the "level density parameter" $a^z$ (multiplied by a constant factor). The ratios of the theoretical values $\Gamma_\gamma^c$ calculated on the basis of the Axel theory to the experimental values $\Gamma_\gamma^e$ are shown in Fig. 18a, while Fig. 18b shows the same for the Weisskopf values (which differ in the powers to which the quantities are raised). Since the theory does not give exact equations, the exponents corresponding to Fig. 18c are empirical. We see that the agreement is not bad and could be improved by taking account of the spin dependence of the radiation width.

The level-density parameter $a$ used in this analysis is calculated from the observed density of resonances. The resonance spacing fluctuates wildly. The statistics of these fluctuations is very interesting and is understood to a large extent; nevertheless, some uncertainty remains, since we cannot be sure that in observing the spectrum we miss some weak resonances especially close to strong ones. With the same

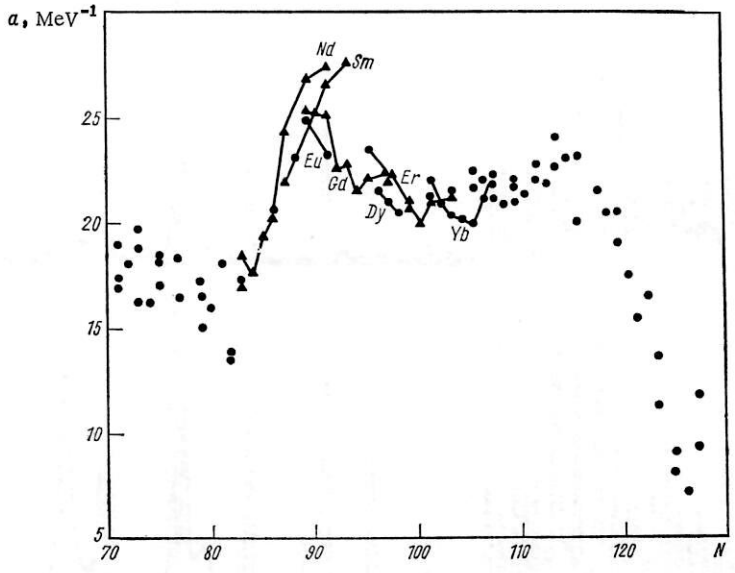


Fig. 19. Dependence of the experimental values of the level density parameter $a$ on the neutron number N.

caveat, we can discuss the average spacing D between resonances, but this is hardly important for a calculation of the parameter $a$, since $a$ is relatively insensitive to large errors in D. Furman and Popov [16] analyzed the values of $a$ on the basis of the experimental level densities, finding peculiar dependences of $a$ on the neutron number. They were able to show that the sharp experimental maximum in $a$ for nuclei having N near 90 (Fig. 19) clearly correlates with the calculated density of one-particle states near the Fermi surface and can be explained on the basis of one-particle states of deformed nuclei. Accordingly, a relationship has been established between the density of one-particle states and the level density of a compound nucleus near the neutron binding energy.

B. Studies of Fissionable Nuclei. Studies of fissionable nuclei can be said to constitute an independent branch of neutron spectroscopy. These nuclei attract the attention of physicists both because of their practical importance and because of the unusual complexity of the fission mechanism. Despite the abundance of experimental information, which is rapidly accumulating, nuclear physics still has not had any striking successes in explaining the physics of fission.

Fission has been studied on the IBR reactor with the maximum baseline of 1000 m, i.e., with a resolution of about 0.05 μsec/m. Figure 20 shows illustrative instrumental curves for the fission (lower curve) and radiative capture (upper curve) of $^{239}$Pu from a few electron volts to several hundred electron volts [17]. Without reviewing all these studies, we simply note that a comparison of these curves after an accurate quantitative normalization yields the quantity $\alpha = \sigma_\gamma/\sigma_f$, of crucial importance in reactor physics. According to the standard experimental procedure, calculations would probably be based on the quantity $\alpha$, even though it would be more natural to use another, equivalent quantity, which might be called the "neutron conversion ratio" $\sigma_\nu$ [18]. This quantity is analogous to that which appears in the resonance integral:

$$\sigma_\nu = (\bar{\nu} - 1)\,\sigma_f - \sigma_\gamma = \sigma_f(\bar{\nu} - 1 - \alpha).$$

Implicitly involved in the use of the quantity $\sigma_\nu$ or $\alpha$ for practical calculations is the assumption that the average number of neutrons per fission $\bar{\nu}$ remains constant. Measurement of $\bar{\nu}$ is of independent interest both for practical purposes and for determining the mechanism for fission. In both cases it is necessary to know how $\bar{\nu}$ depends on the neutron energy and on the nature of the resonance. The quantity $\bar{\nu}$ is in fact constant in a first approximation, but measurements indicate that it may change slightly as a function of the resonance spin. For $^{235}$U these values agree within 3% (those for the $4^-$ states are larger than those for the $3^-$ states), and for $^{239}$Pu (Fig. 21) they agree within 5% (they are greater for the $1^+$ states than for the $0^+$ states). The result reported by Ryabov et al. [19] is at odds with that recorded by Weinstein [20]. The possibility that this discrepancy is due to a difference in experimental procedures was analyzed in [21], but the situation still does not seem to be completely clear.

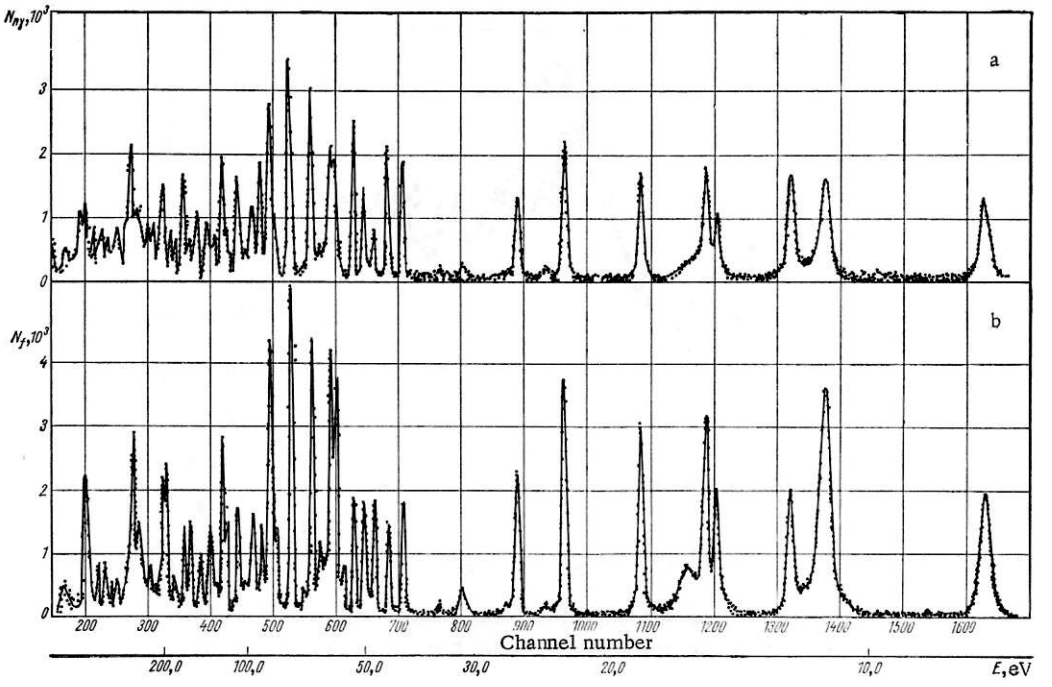


Fig. 20. Instrumental curves for the time-of-flight spectrum for $^{239}$Pu. a) Radiative capture; b) fission.

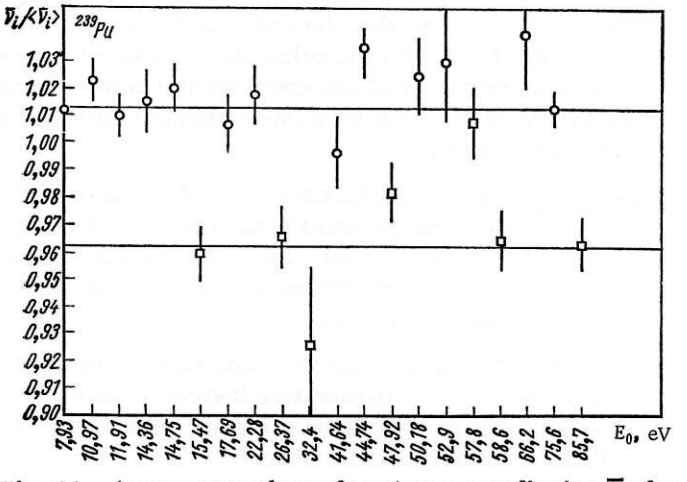


Fig. 21. Average number of neutrons per fission $\bar{\nu}_i$ for $^{239}$Pu resonances divided by the average value $\bar{\nu}_i$ over all the resonances. Circles) Spin-$1^+$ resonances; squares) $0^+$.

For practical purposes, and in view of the accuracy with which $\alpha$ is currently measured, we can assume $\bar{\nu}$ to be constant. In reactor design it turns out to be necessary to determine $\alpha$ for $^{239}$Pu over a wide energy range. This problem has been solved through the efforts of investigators in several countries; measurements carried out with the IBR reactor have been important in this effort.

Figure 22 shows values of $\sigma_f$ measured for $^{239}$Pu from 10 eV to several tens of kiloelectron volts, along with the $\alpha$ values [22]. Interestingly, the fission cross section varies extremely irregularly where the resonances are not resolved and where the curve must have been smoothed considerably. This behavior is evidently due to the feature which was first detected for subthreshold fission. As an illustration, Fig. 23 shows the energy dependence of the subbarrier fission of $^{237}$Np found by Pikel'ner et al. [23], which

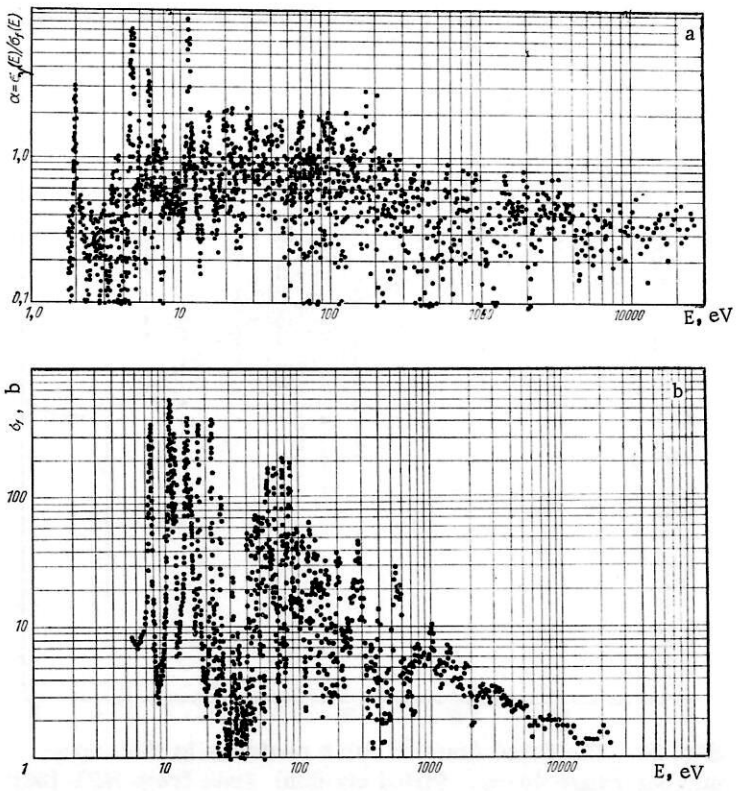


Fig. 22. Fission cross section $\sigma_f$ and the ratio $\alpha$ for $^{239}$Pu.

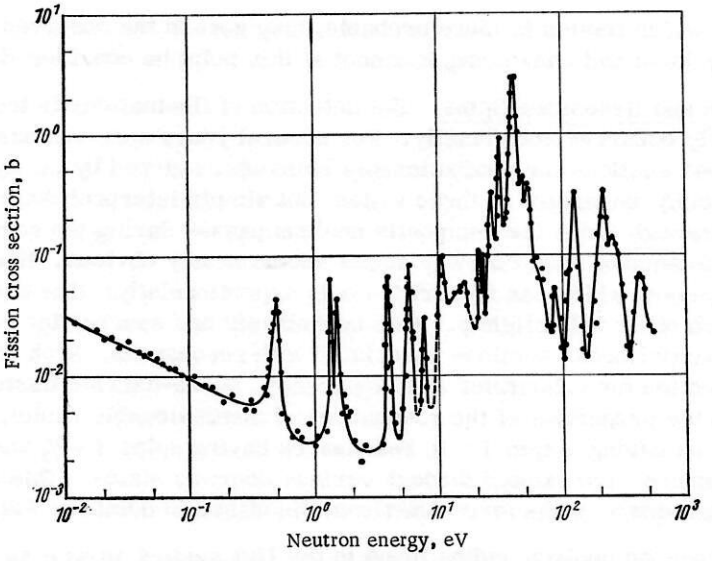


Fig. 23. Neutron-energy dependence of the fission cross section of $^{237}$Np.

agrees with the result found previously at Saclay [24]. In the region in which individual resonances are not resolved (the average spacing is only 0.65 eV), we clearly see peaks in the middle of the fission cross section, at 40, 120, and 250 eV. Such sharp peaks obviously cannot be due to statistical fluctuations in the fission widths of the resonances. They can be explained on the basis of the assumption used, in light of Strutinskii's study, to explain the phenomenon of spontaneously fissionable isomers: that an excited nucleus can display two different types of deformation. A selective probability for a transition to the high-

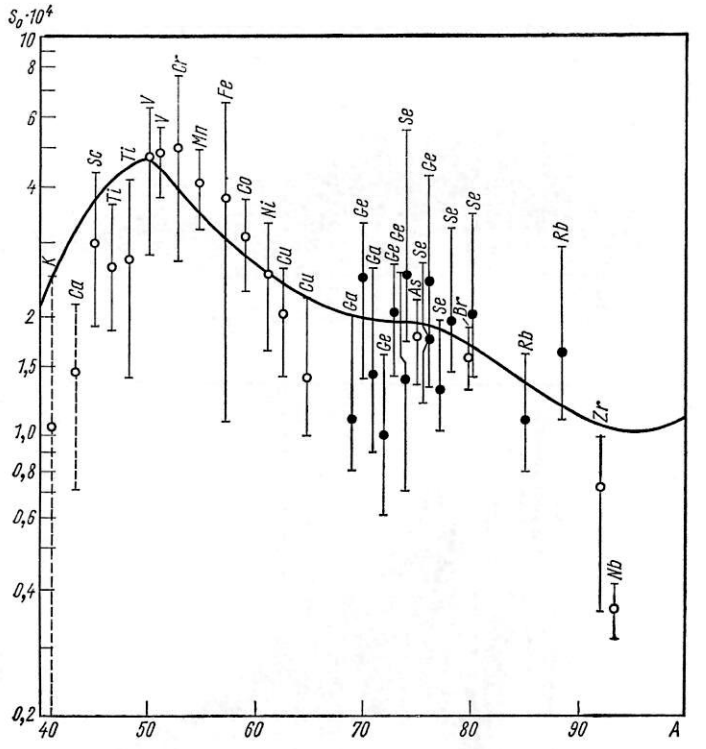


Fig. 24. The force function for s neutrons in the mass-number range 40-90. Filled circles) Data from NPL [26]; solid curve) optical model calculation; open circles) data from the literature.

deformation state, from which fission is more probable, may govern the observed effect. Although this explanation is physically lucid and convincing, it cannot at this point be considered solidly established.

C. Force Function and Resonance Spins. The detection of fluctuations in the cross section for subbarrier fission apparently occurred accidentally. For several years a search has been going on for periodicity in the effective cross sections for nonfissionable elements, spurred by the hypothesis of "doorway states." If we do not specify the nature of these states, but simply interpret them as representing an initial stage of excitation through which the composite nucleus passes during the resonant capture of a neutron, we find that the existence of such doorway states seems nearly obvious. However, an additional hypothesis has been advanced, which can be verified only experimentally: that these doorway states are discrete and overlap each other only slightly. This hyphothesis has spurred the search for periodic changes in the average total or partial cross sections associated with resonances. Such changes have in fact been observed in the cross section for subbarrier and, apparently, above-barrier fission. It is natural to seek analogous phenomena in the properties of the resonances of nonfissionable nuclei. During an s interaction of a neutron with a nucleus having a spin $I > 0$, resonances having spins $I + 1/2$ and $I - 1/2$ are excited. Presumably, these resonances are excited through various doorway states. This possibility has stimulated the search for a spin dependence of the force functions, discussed in detail by Pikel'ner [25].

It is worth noting that the neutron widths found in the IBR studies as well as in other laboratories obey a Porter-Thomas statistical distribution, at least in a first approximation. Accordingly, since only a limited number of resonances have been studied, the force function cannot be determined very accurately. Figure 24 shows the A dependence of the force function in the range from 40 to 90; Fig. 25 shows the same dependence for the range from 120 to 200 [27]. We see that it is difficult to accurately determine the A dependence of the force function, and it is difficult to determine the features of the resonance group on the basis of the neutron widths. We can nevertheless assert that the force function is a relatively stable characteristic of a nucleus, at least in the A ranges shown in Figs. 24 and 25. For gadolinium ($Z = 64$), e.g., the average spacing D between the resonances differs by nearly two orders of magnitude for the two isotopes $^{155}$Gd and $^{160}$Gd (for $^{155}$Gd, we have $D = 1.8 \pm 0.3$ eV, while for $^{160}$Gd we have $D = 170$ eV). The initial

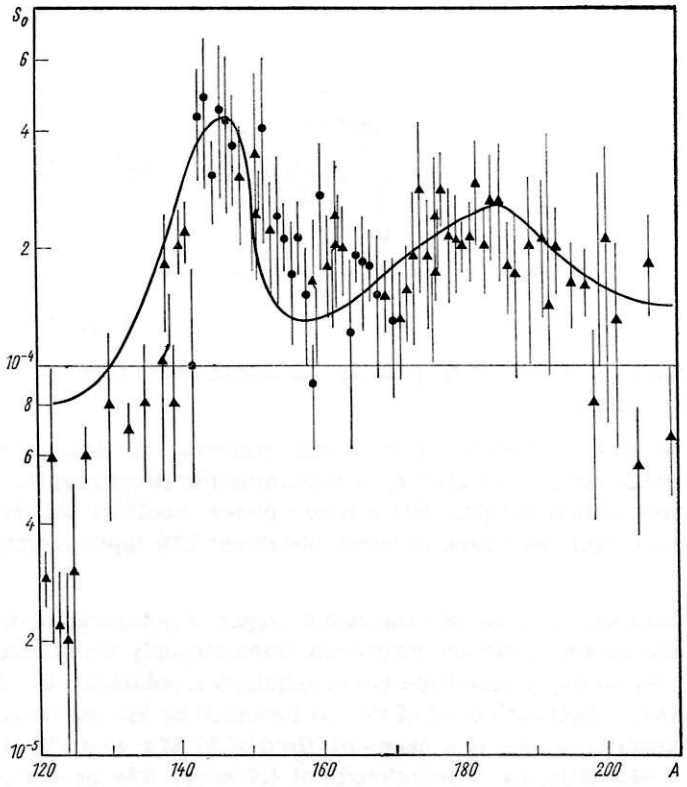


Fig. 25. Force function for s neutrons in the mass number range 120-200. Circles) NPL data; solid curve) optical-model calculation; triangles) data from the literature.

nuclear spins of these isotopes clearly are also different. On the other hand, the respective force functions for these isotopes are $S = (2.1 \pm 0.3) \cdot 10^{-4}$ and $S = (2.6 \pm 1) \cdot 10^{-4}$, i.e., the same, within the experimental error. This agreement might be thought of as a consequence of the theory, but it is more correct to treat it as an experimental fact which shows that the force function is an average characteristic, very insensitive to the individual properties of the nucleus. If these properties are found to have an effect, this discovery would warrant attention. In an analysis of the spin dependence of the force function, Pikel'ner et al. [26] showed that this dependence would be far from simple to detect, and at present there are no reliable data to prove its existence. Accordingly, attention is naturally turned to the individual properties of the resonances, since the possibility is not ruled out that the role of doorway states may be reflected in these properties. It may be that resonances, even those having approximately the same energy and having identical spins and parities, are excited primarily through various doorway states. To solve this problem, we must first determine the resonance spins reliably. It is also extremely important to determine their magnetic moments.

D. Polarized Neutrons and Individual Properties of Resonances. By analyzing neutron-spectroscopy data for samples varying in thickness, we can determine the statistical factor g and thus the spin of a resonance in certain cases. However, this is not possible for many resonances or for a small number of nuclei whose initial spins are small. The spin of a resonance can be determined directly through the use of a polarized neutron beam and a target consisting of polarized nuclei. Such a system, specifically polarized neutrons and polarized protons, has been the subject of study for several years now. In the case of neutrons, however, there has been a difficulty in that the efficiency with which polarized neutrons can be produced by reflection from a nonmagnetic mirror falls off rapidly in the transition from thermal to resonance neutrons. The method proposed by Taran and Shapiro [28] is not afflicted with this problem; it can be used to produce a polarized neutron beam at energies over the entire resonance range. The cross-sectional area of the polarized-neutron beam need not be very small, and the attenuation of the beam by the polarizer is slight.

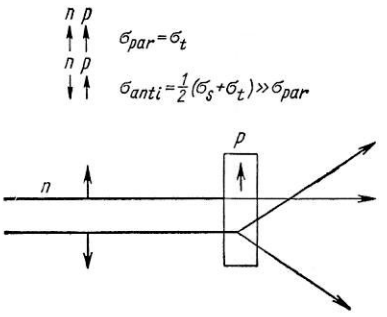


Fig. 26

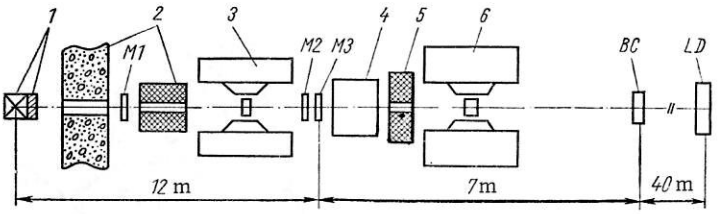


Fig. 27

Fig. 26. Scheme for polarizing neutrons by passing a neutron beam through a polarized target. The arrows show the spin directions.

Fig. 27. Experimental setup for polarized-neutron experiments. 1) Reactor with moderator; 2) biological shielding; 3) polarized proton target; 4) apparatus for reversing the neutron polarization; 5) collimator; 6) polarized nuclear target; M1) reactor-power monitor; M2, M3) monitors for the polarization of the proton target; BC) bank of boron counters; LD) liquid-scintillator neutron detector.

In this method, the neutron beam passes through a target of polarized protons. The neutrons whose spins are antiparallel to the proton spins are scattered more strongly than those having spins parallel to to the proton spins (Fig. 26), so the transmitted beam acquires a polarization. A lanthanum-magnesium titrate crystal [$La_2Mg_3(NO_3)_{12}24H_2O$ with 0.4% of the La replaced by the paramagnetic impurity $^{142}Nd$] is used as polarizer. The target is placed in a magnetic field of 17 kOe at 0.9°K and is polarized by the "solid effect" (an rf frequency of 64.3 GHz, i.e., a wavelength of 4.7 mm). The proton polarization reaches 70%, and with a neutron polarization of about 70% the primary neutron beam is attenuated by a factor of about five. The polarizer has an area of 39 × 31 mm.

This method has been used in neutron spectroscopy to study the spins of the resonances of the holmium nucleus (nuclear spin of I = 7/2) [29]. Holmium was chosen because the large internal magnetic field ($H_{in} = 8.8 \cdot 10^6$ Oe) at 0.3°K in an external field of H = 20 kOe causes the holmium nuclei to have a polarization of several tenths. The experimental setup is shown in Fig. 27, and the results are shown in Fig. 28. The upper curve in this latter figure shows the relative difference between transmissions,

$$\varepsilon = \frac{I_{par} - I_{anti}}{I_{par} + I_{anti}},$$

where $I_{par}$ and $I_{anti}$ are the intensities of the neutrons which pass through the target in the case in which the neutron spin is parallel to or antiparallel to the spin of the Ho nucleus. We see that a change in the sign of the neutron polarization decreases or increases the transmission. We find a qualitative effect here: the sign of the difference between the transmission values unambiguously determines the resonance spin: 4 or 3.

Polarized neutrons have been used successfully to solve another interesting problem, that of determining the scattering length for the scattering of neutrons by deuterium [30]. For many years there has been an ambiguity: there were two sets of scattering lengths (doublet and quartet) satisfying experiment:

$$1)\quad \underline{a_2 = 0.7 \pm 0.3} \qquad \underline{a_4 = 6.38 \pm 0.6}$$
$$2)\quad a_2 = 8.26 \pm 0.12 \qquad a_4 = 2.4 \pm 0.2$$

It was not possible to choose between these sets on the basis of theoretical considerations. Experiments with a polarized deuterium target showed that the first set of scattering lengths, i.e., the quartet length (greater than the doublet region) is correct. Polarized neutrons evidently can also be used to solve several other interesting problems, and they open up some important opportunities. One important application may be in determining the magnetic moments of the resonances. Polarized-neutron experiments have not yet been exploited fully on the IBR reactor, but they are planned, and a methodological study is being carried out.

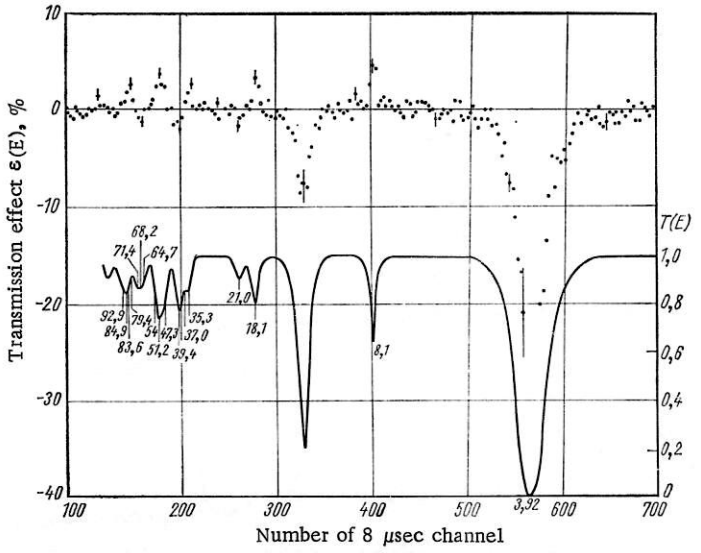


Fig. 28. Measured transmission effect ε for the passage of polarized neutrons through a polarized holmium target (top curve) and transmission T in the unpolarized case (bottom curve).

For example, a cryostat for temperatures down to 0.02°K has been developed for producing polarized nuclei; the lower temperatures are reached by a method developed in the JINR by Neganov (dissolution of $^3$He in $^4$He).

Studies of $\gamma$ spectra excited during the resonant capture of neutrons may furnish an abundance of information about the individual properties of the resonances. Experiments show that the individual properties are displayed very strongly in this case. Experiments by Urbanec et al. [31] have shown that a resonance excited by 24.5-eV neutrons in $^{135}$Ba differs markedly from neighboring resonances (at 82 and 88 eV) in that a $\gamma$ transition to the ground state ($E_\gamma$ = 9.2 MeV) is predominant for it. The difference between the $\gamma$ spectra is so marked that it is difficult to explain by statistical fluctuations in the intensity analogous to fluctuations in the neutron widths $\Gamma_n$. However, the 24.5-eV resonance has a spin different from that of the 82- and 88-eV resonances, and a direct M1 transition to the ground state is possible for it.

The same investigators found an anomalous behavior for Cs resonances [32]. These features can be seen in Fig. 29, which shows the spectra of capture $\gamma$'s measured by a germanium detector for three Cs resonances. Figure 29 shows that the resonance at 47.8 eV is accompanied by a group of $\gamma$ lines at energies from 4.5 to 4.7 MeV, which are not found in the $\gamma$ spectrum resulting from neutron capture by the 22.6- and 5.90-eV resonances. We see from these curves how strongly the individual properties of the resonances are reflected here. In studying these properties of the resonances it is important to search for various types of correlations, e.g., between neutron widths and partial $\gamma$ widths. For this reason there is considerable interest in the correlation inferred from Brookhaven experiments between the probability for the emission of hard $\gamma$'s and the neutron width of the resonances. Whether this behavior directly reflects the existence of doorway states evidently cannot be determined on the basis of the experimental results available, but the outlook for progress in this field seems very promising.

Another field in which much information can be found about the individual properties of resonances is study of the $\alpha$ decay of neutron-excited resonances. The probability for this type of resonance decay, found by Popov and Kvitek in 1966 for Nd and Sm isotopes [33], is less than 0.001% of the probability for radiative capture. Improvements in the experimental procedure, however, led to a determination of not only the total width corresponding to this type of decay, but also the $\alpha$ spectra, i.e., the probabilities for $\alpha$ decay to the ground and certain excited states. Since this method is simple, and since the mechanism for $\alpha$ decay is well understood, this method is extremely promising, even though it cannot be used for many nuclei. A more detailed analysis of this topic, by Yu. P. Popov, appears elsewhere in this series, and Solov'ev [34] has discussed certain theoretical aspects of this problem.

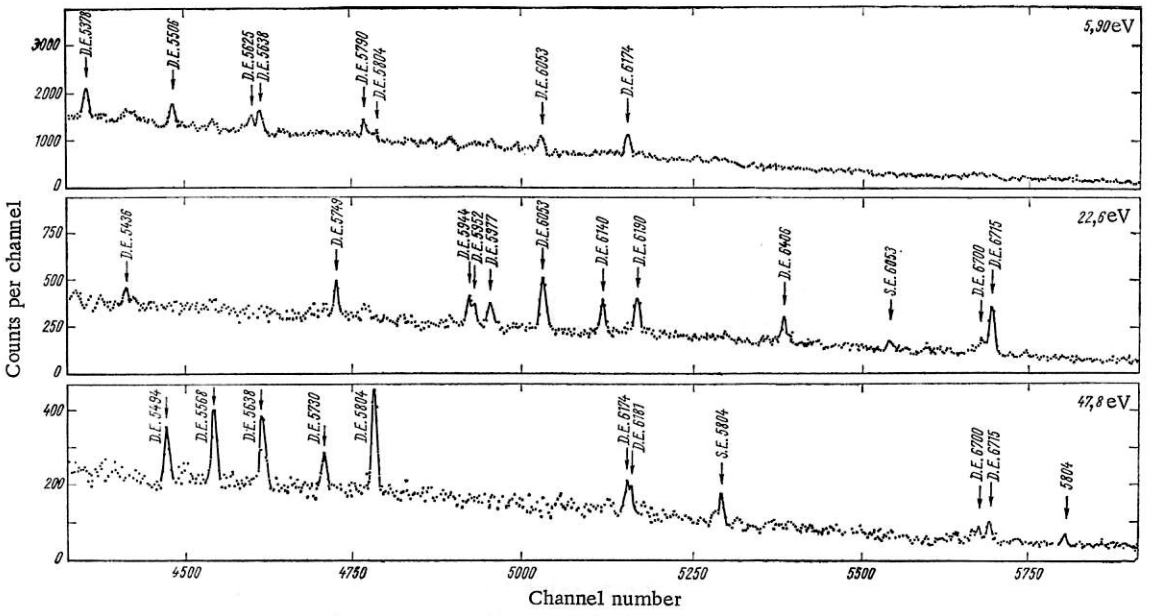


Fig. 29. Spectra of Cs $\gamma$'s during neutron capture at the 5.90-, 22.6-, and 47.8-eV resonances.

## 3. Experiments with Thermal and Cold Neutrons

The length of the neutron pulse in the IBR reactor, about 60 $\mu$sec, is comparable to the characteristic time for the emission of delayed neutrons by the hydrogenous moderator (~100 $\mu$sec). Accordingly, the IBR reactor can be used for time-of-flight studies with thermal and cold neutrons. On the basis of the relatively little information available in the literature at the time of the IBR start-up (1960), it was natural to begin the study with the problem of the inelastic interactions of cold neutrons separated by means of a beryllium filter. Development of a procedure for these experiments, carried out primarily by Golikov and Shkatula, was begun in 1960 during the start-up work. The first study was made of inelastic scattering of neutrons in water; this study was stimulated by an interesting study by Hughes et al. [35] which appeared just prior to that time. At that time, however, there had been little experience in this type of measurement in any laboratory, so some time was required in order to obtain reliable results. A pattern was found in the results, which were summarized in a report by Golikov et al. to the Symposium on Inelastic Scattering of Neutrons, held in Bombay in 1964 [35]. The results of a study of ice and water at various temperatures as well as of certain organic liquids were reported. The experimental procedure, however, was not suitable for the neutron source used. The experimental setup is shown in Fig. 30.

The sample was placed in the reactor room behind a beryllium filter which was pressed against the active-zone moderator. Since the scattered beam had to be taken out through an existing channel in the shielding, and it was difficult to reach the sample, it was difficult to adjust the scattering angle. Accordingly, a change was made of the backward geometry (Fig. 31), which became the predominant setup.

In this setup the energy of the neutron incident on the sample is arbitrary and is determined from the time which elapses during the neutron flight from the reactor to the sample (more precisely, to the detector, which is adjacent to the sample), but the final neutron energy is fixed, because a beryllium filter which transmits only cold neutrons is placed in front of the detector. In order to achieve an adequate baseline, the sample is quite distant from the reactor (~20-30 m), i.e., necessarily outside the reactor room. Under these conditions there is no problem in adjusting the experimental conditions (replacing samples, changing the temperature, changing the scattering angles, etc.). This method has the further advantage that inelastic scattering involving a transfer of energy to the material can be studied; i.e., the frequency spectrum is not limited by excitations in the material. The backward-geometry setup was first used independently by Machekhina et al. [36], although slightly later than by other investigators (e.g., R. Sinclair in 1961). Figure 32 shows one series of experimental curves, obtained for $NH_4Cl$ at various temperatures [37]. Here the detector count is shown as a function of the time of flight, so the right sides of the curves correspond to the lowest energies, i.e., to cold neutrons, to which the beryllium filter is transparent. This

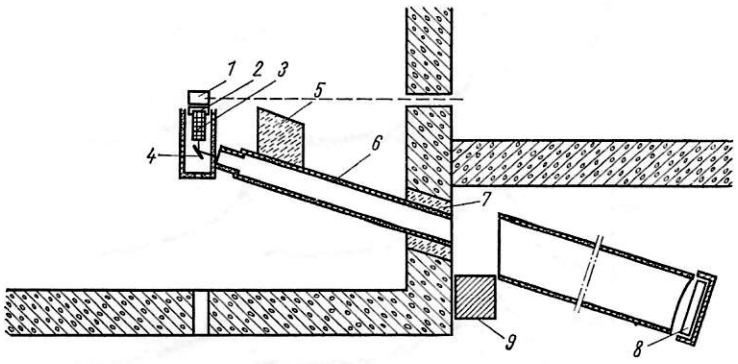


Fig. 30. Experimental setup for studying inelastic neutron scattering in the forward geometry. 1) Active zone of reactor; 2) moderator; 3) beryllium filter; 4) sample; 5) shielding from direct beam; 6) neutron duct; 7) water shielding; 8) detector; 9) slide valve.

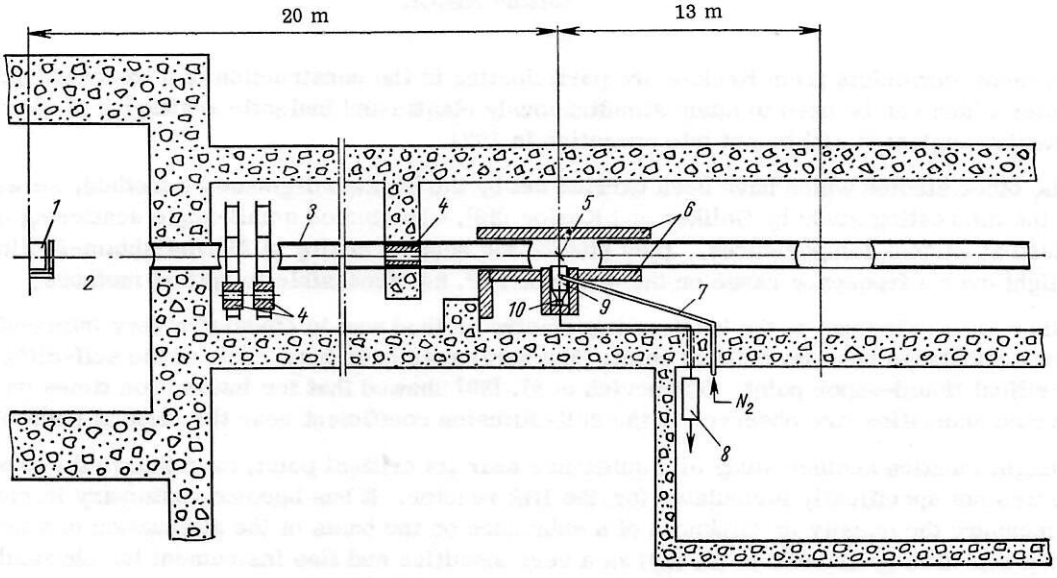


Fig. 31. "Backward-geometry" setup for an experimental study of the inelastic scattering of neutrons. 1) Active zone of reactor; 2) moderator; 3) neutron duct; 4) collimators; 5) sample; 6) shielding; 7) nitrogen pipe; 8) electronics for detector; 9) cooled beryllium filter; 10) detector.

part of the spectrum is governed by quasielastic neutron scattering, during which the neutron energy changes little. The high-energy spectrum of such neutrons, i.e., that corresponding to the short flight times, is limited by the transmission of the beryllium filter, which becomes opaque to neutrons at $E > E_{1i} = 5.2$ MeV. All the curves show a sharp cutoff of the spectrum at $E = E_{1i}$. At the left in Fig. 32 is the region of inelastic scattering of neutrons; before the scattering these neutrons have energies above $E_{1i}$, so the corresponding flight times are shorter.

The backward-geometry experiments were carried out for several years under the supervision and with the participation of professor Janik (from Krakow). Several improvements were made in the procedure; in particular, the resolution was improved by combining a beryllium filter with a crystal spectrometer, which limited the transition to a narrow range near $E_{1i}$. The backward-geometry method was used for a broad range of studies of the dynamics of molecular-crystal excitations, in determining the dynamics of the excitations of binary alloys, and in several other fields; in particular, the effect of light impurity atoms was determined.

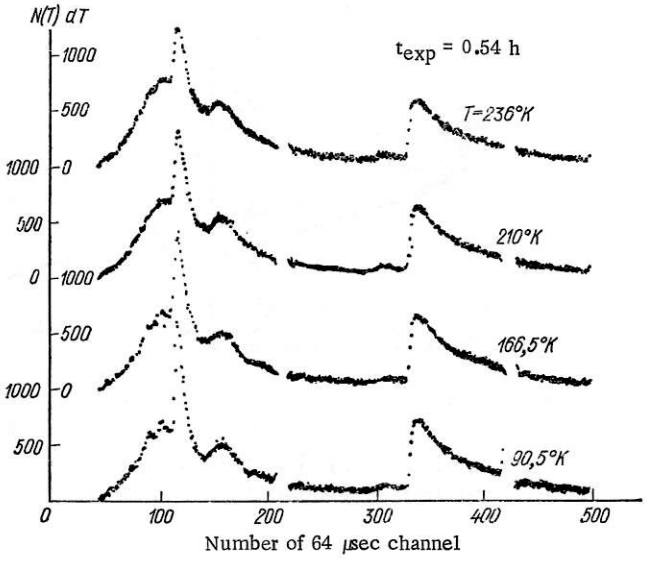


Fig. 32. Spectrum of neutrons scattered by polycrystalline $NH_4Cl$.

At present, physicists from Krakow are participating in the construction of a backward-geometry spectrometer which can be used to study simultaneously elastic and inelastic scattering of slow neutrons at eight scattering angles; it will be put into operation in 1971.

Of the other studies which have been carried out by the backward-geometry method, we will mention here only the interesting study by Golikov and Kozlov [38], who studied small-angle scattering of slow neutrons by lead at various temperatures. They studied the neutron analog of Mandel'shtam-Brillouin scattering of light over a frequency range on the order of $10^{12}$, not accessible to optical methods.

Another interesting use of the backward-geometry method was in studying a very interesting problem: the state of a substance near its critical point. Measurements have been made of the self-diffusion of ethane near the critical liquid-vapor point. Ostanevich et al. [39] showed that for interaction times on the order of $10^{-12}$ sec no anomalies are observed in the self-diffusion coefficient near the critical point of ethane.

We might mention another study of a substance near its critical point, even though the experimental procedure was not specifically formulated for the IBR reactor. It has become customary in modern technology to measure the density or thickness of a substance on the basis of the attenuation of a neutron beam. This method was used by Bulavin et al. [40] as a very sensitive and fine instrument for physical research. It has been used to measure the density of ethane near the critical point.

In studying inelastic scattering of neutrons it is very useful to have the capability of bombarding the substance with a monoenergetic neutron beam and of determining, at various scattering angles, the entire spectrum of neutrons produced in the inelastic interaction. This complex problem was solved in a study carried out at the NPL by Soviet physicists from the Physicoenergetic Institute [41]. The apparatus operates in the following manner (Fig. 33): The neutron beam from the IBR reactor is cut off at a distance of about 10 m by a mechanical selector operating in synchronism with the reactor. The energy of the neutrons transmitted by the selector is determined from the time which elapses between the reactor pulse and passage through the selector. The selector thus operates as a monochromator. The spectrum of neutrons scattered by the sample is analyzed on the basis of the time of flight at 11 angles simultaneously and over baselines of 5.5 to 10.5 m. Figure 34 shows the experimental room; in the background are water-filled tanks offering shielding from the background of various beams of scattered neutrons. This apparatus has been used for a wide-ranging study of inelastic scattering of slow neutrons by zirconium hydride.

The neutron-diffraction method is a traditional method for atomic-reactor experiments. Such studies of the structure of condensed media have been successfully carried out in beams of steady-state reactors, and it was not immediately obvious whether the pulsed nature of the IBR reactor would be important, or whether only the average neutron flux (not very high for the IBR) would be important. From the very be-

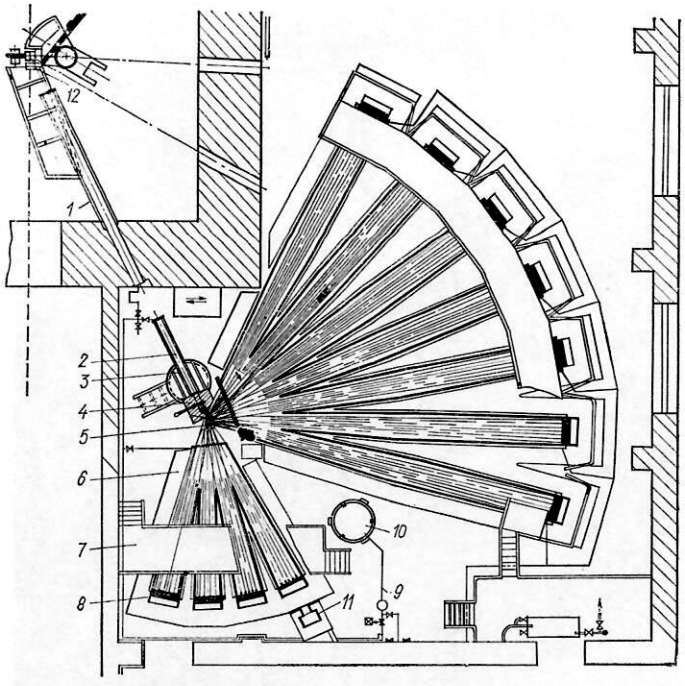


Fig. 33. Double differential spectrometer for slow neutrons. 1, 2) Neutron ducts; 3) rotating circle; 4) chopper; 5) 10.5-m neutron duct; 6) 5.5-m neutron duct; 7) pier; 8) detector; 9) gas system; 10) gas tank; 11) neutron trap; 12) cryostat.

ginning it was obvious in the discussion of studies planned for the NPL that there was no need to monochromatize the neutrons diffracted at a given angle, since the various neutrons satisfying the Bragg have different velocities and are distinguishable on the basis of the flight time.

Later, the method of neutron diffraction on the basis of flight was given experimental and theoretical bases by the work of Warsaw physicists guided by professor Buras [42] and of Soviet physicists (Nitts et al. [43]). The essence of the method is well known, so we will mention here only those points that are required for this discussion. For simplicity we assume that a polycrystalline sample is being studied, so for given directions of the incident and scattered beams there are always corresponding reflection planes for which the angles of incidence and reflection are equal. Then it is simply necessary to satisfy the Bragg condition, which takes the following form when the wavelength is expressed in terms of the velocity:

$$2d \sin \theta = n\lambda = nh/mv.$$

For a given $\theta$ each d and n determine a value of v. For fixed baselines $L_r$ and $L_c$ from the reactor to the sample and from the sample to the detector, respectively, and for a given $\theta$, each d and n thus correspond to a particular flight time. The Bragg relation can evidently be rewritten as

$$v \sin \theta \cdot d = v_z d = n \left( \frac{h}{2m} \right).$$

Here $v_Z$ is the projection of the neutron velocity on the normal to the reflection plane.* For the time of flight, we can write

$$t = (l_r + l_c)/v_z.$$

* If the scattering angle is specified exactly, the normal to the reflection plane obviously coincides with the bisector of the angle between the source-sample line and the detector-sample line.

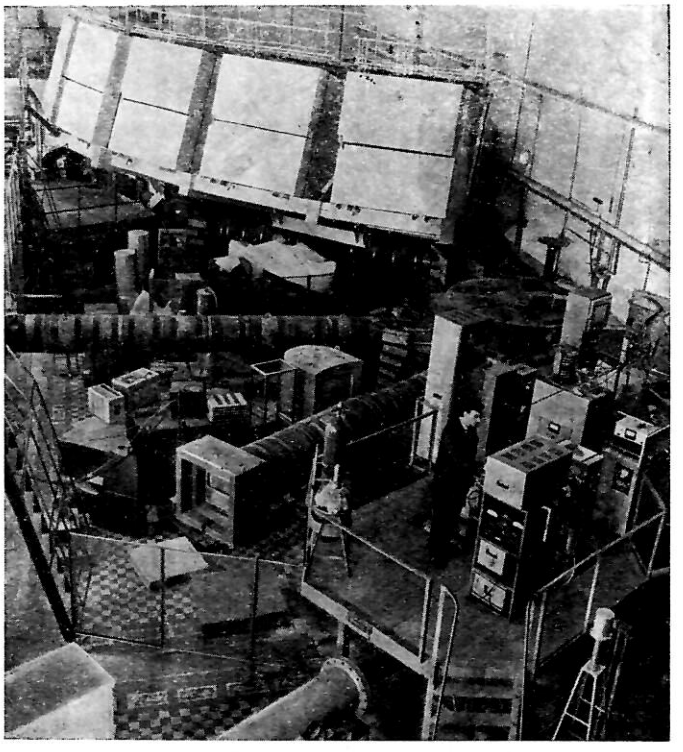

Fig. 34. The experimental room. In the foreground is the apparatus used to produce the polarized neutrons; behind it is the apparatus with the double differential spectrometer. Water-filled tanks shielding the detectors are also visible.

where $l_r$ and $l_c$ are the projections of $L_r$ and $L_c$ on the normal to the reflection plane (see Appendix 3). It follows immediately that there is no need to collimate the beams of incident and reflected neutrons; it is simply necessary that the sum of the projections $l_r$ and $l_c$ remain constant. This condition is easily satisfied. We could also require that sum $l_r + l_c$ remain constant for all reflection planes in some angular interval $\Delta\theta$, rather than for some particular angle: at the angular position of the reflection plane, $l_r$ may increase and $l_c$ decrease, or vice versa, in such a manner that their sum remains constant. The simplest case $L_r = L_c$, used as an example in Appendix 3, can be understood clearly without a mathematical analysis. This is a particular case of the general relations found by Holas in a series of studies begun in 1966 and which have been verified experimentally [44] (Appendix 3).

Since the beam collimation characteristic of the ordinary diffraction method is eliminated here, the time-of-flight method can be used at relatively high intensities. It also seems significant that in a polycrystalline sample there are contributions to the diffraction from planes occupying a finite angular range; again, the flux intensity available is increased. Figure 35 shows one of the experimental geometries designed on the basis of the Holas method. A series of studies of time-of-flight neutron diffraction have shown it to provide relatively high fluxes and a good resolution [45]. Without going into these studies in detail, we will point out two approaches which go beyond the framework of classical neutron-diffraction experiments. Because of the brief intense pulse of neutron radiation, the IBR reactor can be used to study, in addition to the structure of matter by the diffraction method, the structural changes which occur during the pulse. In the first use of this approach, a study was made of the behavior of the diffraction peak of magnetic neutron scattering in hematite subjected to an intense pulsed magnetic field. The very first experiments showed an anomalous behavior of magnetic scattering in a field of about 50 kOe. This study was carried out by a large group of investigators [46]. A more detailed study of this anomalous behavior is currently under way.

Another field in which the neutron-diffraction method has turned out to be unexpectedly promising is the physics of elementary particles. The neutron is a very convenient object for experiments in this

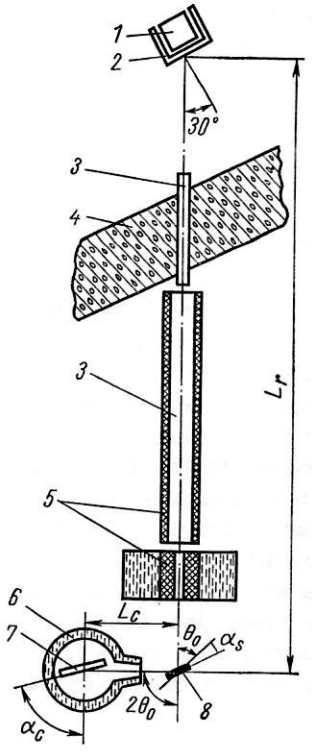


Fig. 35. Experimental setup for time-of-flight neutron diffraction. 1) Active zone of reactor; 2) moderator; 3) neutron duct; 4) concrete shielding; 5) paraffin with boron carbide; 6) water shielding; 7) detector; 8) sample.

field, since its lack of an electric charge allows experiments with beams of low-velocity particles. One interesting problem, the neutron-electron interaction, is being studied by Aleksandrov and Samosvat; since the topic is discussed in detail in [47], here we will simply give a brief description of the formulation of the problem. The interaction of a neutron with the electronic shell of an atom is a very weak interaction in comparison with the nuclear interaction. On the other hand, in scattering of neutrons by nuclei one must take into account not only potential and resonance scattering, but also their interference. It turns out that there is an isotope for which the nuclear scattering amplitude nearly vanishes due to an interference between resonance and potential scattering: $^{186}W$. This scattering is so weak that a $^{186}W$ single crystal must be used, and the diffraction peak due to the coherent superposition of the scattering amplitudes of many atoms must be observed. It has also been learned that, in principle, the addition of a slight impurity of other tungsten isotopes to a $^{186}W$ crystal can result in a vanishing nuclear scattering amplitude. Such a tungsten crystal should display the same diffraction pattern as in the case of x rays, since the entire interaction must be governed by scattering by the electronic shell of the atom. Accordingly, account of the nuclear properties of $^{186}W$ and the use of neutron diffraction have turned out to be fruitful for solving an interesting problem in the physics of elementary particles. Measurements which have been carried out show completely convincingly that interference of electronic and nuclear scattering can be observed. However, it is possible that some other factor is not taken into account in the interpretation of the results. Although the result found for the electronic scattering was found to be on the expected order of magnitude (corresponding to an interaction potential of $V_0 = -6500$ eV), it is slightly greater than the results found by other methods ($V_0 = -3000$ to $-5000$ eV). This discrepancy evidently requires further analysis.

The same intertwining of problems and methods is observed in other topics in the physics of elementary particles. For example, a study of the angular distribution of neutrons as a function of the neutron energy over the range 1-40 keV carried out by Aleksandrov and Samosvat [48] is interesting from two points of view: for the physics of elementary particles and for nuclear physics. The isotropy of the neutron scattering corresponding to an s interaction should give way as the energy is increased. Theory predicts that at low energies the basic contribution to the anisotropy comes from a term proportional to the cosine of the angle, and the coefficient of this term should be proportional to the energy. This dependence was studied by Aleksandrov and Samosvat [48] and confirmed experimentally for several nuclei. The results obtained were compared with those calculated on the basis of the optical model.

In certain cases, however, anomalies are observed; e.g., lanthanum does not display a linear dependence. These results, especially the anomalous ones, are interesting in connection with nuclear physics. On the other hand, analysis of the angular distribution of the scattering and its energy dependence allows a significant lowering of the upper limit on the possible electric polarizability of the neutron [47].

The last topic, which we will discuss very briefly, is that of ultracold neutrons. This field can be said to have begun with the experimental detection of such neutrons in 1968 by a group of physicists under the guidance of professor F. L. Shapiro [39]. Although the properties of these neutrons were predicted by Zel'dovich [50] more than a decade prior to that time, the verification of these properties was surprising and upset some supposedly final conclusions which had been reached about the neutron. It is unusual that the gravitational force confines ultracold neutrons in a layer no longer than 2 m and that they are reflected nearly ideally from the surfaces of many substances, so they can be stored in a closed volume for a long time.

The pulsed nature of the IBR reactor has turned out to be a great advantage for detecting ultracold neutrons. The experimental procedure is simplified because neutrons can be observed during the interval

between pulses, at which time the parasitic background is negligible. The number of ultracold neutrons, governed by the relatively small average flux of thermal neutrons from the IBR reactor, was extremely small (about one neutron per 100 sec was detected). However, the possibility of storing ultracold neutrons in a cavity with reflecting walls allows us to hope for a significant increase in the density of ultracold neutrons when a periodic pulse source is used. When a reflecting gate is opened during the reactor pulse and closed for the rest of the time, the neutron density in a cavity in which neutrons are stored ideally will increase until the density reaches the value governed by the peak flux of neutrons from the reactor, rather than by the average flux. Preparations are currently under way for such experiments on the IBR reactor.

A study of the time for which ultracold neutrons can be stored in a reflecting cavity and of the energy spectrum of such neutrons was recently carried out jointly by the NPL and the Kurchatov Institute of Atomic Energy [51] at the steady-state reactor of the Institute. The neutron density in a cavity having polished-copper walls decays with a time constant of about 30 sec; such a long time is extremely rare in neutron physics and is thus very interesting. On the other hand, this time is shorter than that calculated on the basis of the expected absorption of these neutrons in the copper, and the reason for the discrepancy is not clear. Very ingenious experiments, in which these neutrons were transmitted through an elbow, in which they could only rise to a given height or drop, revealed the spectrum of these neutrons. The spectrum corresponds to the lower end of a Maxwell distribution and for copper extends to a maximum velocity of $v_{max}$ = 5.7 m/sec, which corresponds to a value of 1.65 m for the maximum height which they can overcome. Only the first steps, of course, have been taken in the study of ultracold neutrons, but it is not too soon to discuss their applications in elementary-particle physics and in studying surface layers of materials and, for the future, to discuss the development of their optics. A possible problem for the future is the design of a neutron microscope.

## CONCLUSION

To summarize this paper, we note that a decade's use of the IBR reactor and the injector-equipped reactor have shown the fruitfulness of this investigative tool for a wide range of problems in nuclear physics, elementary-particle physics, and the physics of condensed media. It is hoped that in this manner the practical limit of $10^{15}$ neutrons/(sec · cm$^2$) on the neutron flux density typical of steady-state reactors can be overcome.

In discussing future research, we wish to emphasize the bright outlook for studies with polarized neutrons for solving many problems. It also seems useful to study the spectra of $\gamma$'s produced in the resonance capture of neutrons and to study the $\alpha$ decay of neutron resonances, in order to obtain a wide variety of information about the properties of the various resonances.

Through the use of inelastic neutron interactions and neutron diffraction, it seems possible to solve a wide variety of physical problems, especially in the physics of condensed media. Particularly promising here is the study of the dynamics of processes in a substance for which the pulsed nature of the neutron source has important advantages. There will probably also be applications in studying the structure and frequency spectra of biological molecules.

An extremely broad research field deals with the properties of the neutron itself. In the case of ultracold neutrons there is obvious interest, and the applications of these neutrons will be determined in the future.

The author thanks L. B. Pikel'ner for preparing this paper for publication and L. B. Pikel'ner and F. L. Shapiro for useful comments offered in discussion of this paper.

## APPENDIX 1

### Basic Relations from the Theory for the IBR Reactor

We assume that for the optimum position ($x = 0$) of a moving active insert in a disc or rotating reflector, the maximum reactivity for prompt neutrons is

$$\varkappa_{max} = \varepsilon = K_{max} - 1. \quad (1)$$

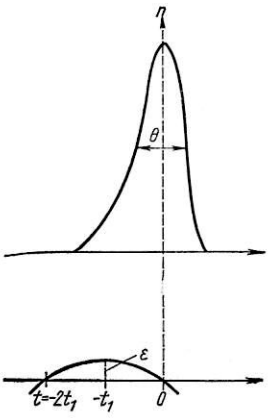


Fig. 36. Time dependences of the reactivity ε and the number of neutrons n.

As the insert or reflector moves, the reactivity changes quadratically; i.e., the reactivity decreases by an amount $\alpha x^2$ as a result of a displacement by x. We denote by v the displacement velocity, and we choose as the time origin t = 0 the instant at which the reactivity passes through zero after its peak (Fig. 36):

$$\varkappa = \varepsilon - \alpha x^2 = \varepsilon - \alpha v^2 (t + t_1)^2; \quad t_1 = \frac{\varepsilon^{1/2}}{v\alpha^{1/2}}; \tag{2}$$

$$\varkappa(t) = -\alpha v^2 t^2 - 2\alpha^{1/2} \varepsilon^{1/2} vt. \tag{3}$$

The maximum reactivity occurs at time $t = -t_1$, and the reactivity remains positive from $t = -2t_1$ to t = 0 (Fig. 36). Throughout this interval the reactor power evidently increases due to a chain reaction involving prompt neutrons and reaches a maximum at t = 0.

When the reactor power is sufficiently high, the development of a power pulse is described by

$$\ln \frac{n(t)}{n_0} = \int_{-2t_1}^{t} \frac{\varkappa(t)}{\tau} dt. \tag{4}$$

where $\tau$ is the average lifetime of fast neutrons in the reactor (Appendix 2). Equation (4) holds if the entire chain reaction involves prompt neutrons and if n is so large that the constant source of delayed neutrons can be neglected. As Shabalin has shown, this condition does not hold for a time interval near $t = -2t_1$, i.e., near the lower integration limit. Accordingly, in order to obtain the correct pulse amplitude near t = 0, which will be used below, we must set $n_0$ in Eq. (4) equal to roughly twice its actual value at the time $t = -2t_1$. Substituting $\varkappa(t)$ from Eq. (3) into Eq. (4) and integrating, we find the basic equations of the Bondarenko-Stavisskii theory:

$$n(t) = n_0 \exp\left(\frac{4}{3} B - \frac{t^2}{\theta^2} - bt^3\right), \tag{5}$$

where

$$B = \frac{\varepsilon^{3/2}}{\tau v \alpha^{1/2}}; \quad b = \frac{1}{3} \cdot \frac{\alpha v^2}{\tau}; \tag{6}$$

$$\theta = \frac{\tau^{1/2}}{\alpha^{1/4} v^{1/2} \varepsilon^{1/4}} = \frac{\tau^{1/3}}{B^{1/6} v^{2/3} \alpha^{1/3}}. \tag{7}$$

The maximum intensity at t = 0 is evidently

$$n_{max} = n_0 \exp\left(\frac{4}{3} B\right). \tag{8}$$

Near t = 0 the n(t) dependence can be represented approximately by a Gaussian curve having a width $\theta$. We see from Eq. (7) that in the first approximation ($B^{1/6}$ = const), the quantity $\theta$ is governed by the reactor constants $\tau^{1/3}$ and $\alpha^{1/3}$ and by the velocity $v^{2/3}$. In addition, it depends slightly on the maximum supercriticality $\varepsilon$. The value of $\varepsilon$ is not arbitrary. In order for the reactor to operate in the steady state, i.e., in order for the average pulse amplitude to be constant, we must have $\varepsilon = \varepsilon_0$, where $\varepsilon_0$ is the pulsed criticality, discussed below. Accordingly, the value of $\theta$ at v = const is nearly independent of the reactor power. We see from Eq. (5) that the pulse shape is slightly non-Gaussian because of the term $-bt^3$ in the exponential function (the rise is slower than decay). Figure 37 shows the experimental pulse shape for the IBR-30 reactor along with the shape calculated from Eq. (5) on the basis of the actual values of v, $\tau$, and $\alpha$. We see that near the pulse peak, where the theory is correct, the agreement is quite good.

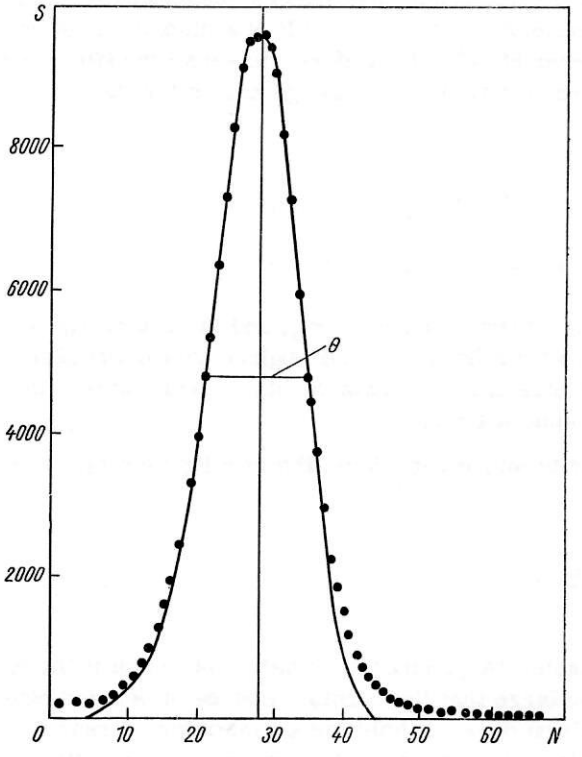


Fig. 37

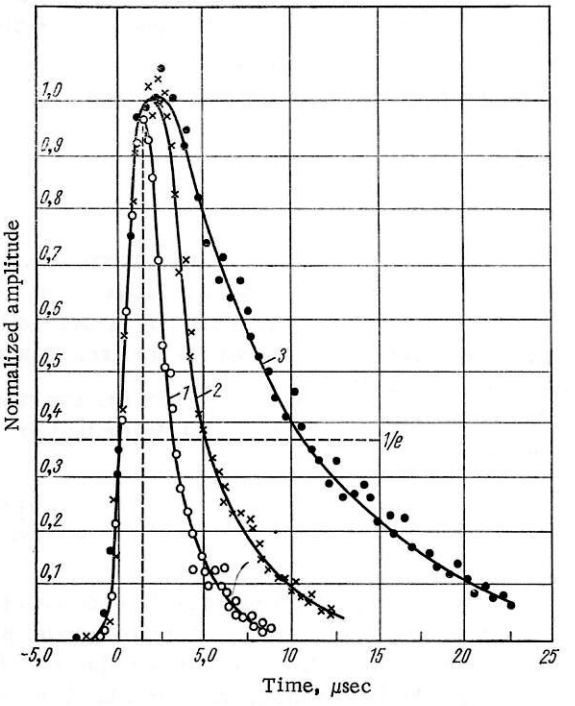


Fig. 38

Fig. 37. Experimental shape of the reactor pulse (points) and that calculated from Eq. (5) (curve).

Fig. 38. Pulse shape for the injector-equipped reactor for various k: 1) k = 120, W = 25 W, $T_{1/2}$ = 2.5 μsec, $\tau$ = 2 μsec, $\tau_{calc}$ = 1.5 μsec; 2) k = 300, W = 60 W, $T_{1/2}$ = 4.0 μsec, $\tau$ = 3.8 μsec, $\tau_{calc}$ = 3.6 μsec; 3) k = 1000, W = 200 W, $T_{1/2}$ = 9.0 μsec, $\tau$ = 10 μsec, $\tau_{calc}$ = 12 μsec.

The neutrons which trigger the pulse are delayed neutrons $n_d$. The value which should be used as the initial value in Eq. (5) (i.e., $n_0$), is proportional to $n_d$: $n_0 = a_0 n_d$, where $a_0$ is some coefficient which is proportional to the multiplication of delayed neutrons at the beginning of the pulse. If the decay in the intensity of delayed neutrons during the time T between pulses is slight, the number of neutrons per pulse is

$$N_d = n_d T. \tag{9}$$

The number of prompt neutrons produced per pulse is given approximately by [see Eq. (8)]

$$N_{prm} \approx n_{max}\theta = \theta a_0 n_d \exp\left(\frac{4}{3}B\right). \tag{10}$$

During steady-state operation of the reactor, under which conditions we have $\varepsilon = \varepsilon_0$, we must have

$$N_d = \beta N_{prm}, \tag{11}$$

where $\beta$ is the effective relative number of delayed neutrons per prompt neutron.

Using $N_d$ and $N_{prm}$ from Eqs. (9) and (10), we find an equation for B and thus [see Eq. (6)] the pulsed criticality $\varepsilon_0$:

$$\ln\frac{T}{a_0\beta\theta} = \frac{4}{3}B = \frac{4}{3}\cdot\frac{\varepsilon_0^{3/2}}{\alpha^{1/2}v\tau}. \tag{12}$$

For a given v the quantity $\varepsilon_0^{3/2}$ thus has an approximately ln T dependence on the pulse repetition period.

Experimentally, an important consideration is the neutron background from the reactor in the interval between pulses:

$$n_b = k_0 n_d, \tag{13}$$

where $k_0$ is the multiplication coefficient for delayed neutrons between pulses; for the IBR reactor, we have $k_0 \approx 14$. Using Eqs. (11) and (9), we can rewrite Eq. (13) as

$$n_b = k_0 \frac{\beta}{T} N_{prm}, \tag{14}$$

Accordingly, the background-neutron flux is proportional to $N_{prm}$ and $1/T$.

During operation with the injector, the reactor is used in the booster mode, in which the maximum reactivity is negative; $\varkappa_{max} = k - 1 < 0$. The neutrons are injected at the instant at which the equality $\varkappa = \varkappa_{max}$ occurs, and neutron multiplication occurs. The number of neutrons tends toward the value $n = n_p(1 - k)$, where $n_p$ is the number of neutrons produced by the injector. When the neutron pulse from the injector ends, the number of neutrons begins to decay exponentially, as $\exp(-t/\tau_1)$, where $\tau_1 = \tau/(1 - k)$. The total pulse length is thus governed by the length $\tau_0$ of the accelerator pulse; the decay requires a longer time for greater neutron multiplication. Figure 38 shows the pulse shape produced by the IBR reactor operated with the microtron injector for various k. For this reactor we have $\tau = 1.2 \cdot 10^{-8}$, so for a multiplication of 100, i.e., for $1 - k = 10^{-2}$, we find $\tau_1 \approx 1$ μsec. Interestingly, while the decay in the reactor operated without the injector is governed by a Gaussian law, it is exponential when the injector is used, so for large multiplications we find a slowly decaying exponential tail. With $\tau \approx 10^{-8}$ sec, a multiplication of 100-200 corresponding to $\tau_1 \approx 1$-2.5 μsec turns out to be optimum for experiments. The optimum length $\tau_0$ of the current pulse from the accelerator should be on the same order of magnitude.

## APPENDIX 2

### Some Information about the Development and Parameters of the IBR Reactor

The IBR Reactor. The first IBR reactor reached pulsed criticality on June 23, 1960. It had the following parameters:

Design power of $\bar{W} = 1$ kW,
Pulse length of $\theta = 36$ μsec,
Average neutron lifetime of $\tau = 1.2 \cdot 10^{-8}$ sec for a single generation,
Pulse repetition frequencies of $f = 8.8$ and 83 $\text{sec}^{-1}$
(rotation velocity of 5000 rpm for the primary disc),
Actual average reactor power of:
for 1961-1963, $\bar{W} = 1$ kW,
for 1964, $\bar{W} = 2$-6 kW,
for 1965-1968, $\bar{W} = 3$ kW.

When the power was reduced to 3 kW the disc rotation velocity was reduced to 3000 rpm. The pulse length turned out to be $\theta = 50$ μsec, and the pulse repetition frequencies were $f = 3.3$, 5, and 50 $\text{sec}^{-1}$. The average neutron flux into a solid angle of $4\pi$ at 3 kW was $N = 1.7 \cdot 10^{14}$ neutrons/sec. With $f = 3.3$ $\text{sec}^{-1}$ and $\bar{W} = 3$ kW the maximum power is $W_p = 18$ MW. The resolution of the neutron spectrometer with a base line of $L = 10^3$ m was $r = \theta/L = 0.05$ μsec/m.

Operation in the isolated-pulse mode was begun in 1968, with $f = 1/5$ $\text{sec}^{-1}$ and $W_p = 10^6$ kW. The pulse length was reduced to $\theta = 36$ μsec. The 30-MeV microtron injector was put into operation in 1964, at a pulsed current of 50 mA. With $f = 50$ $\text{sec}^{-1}$ and a multiplication of $N/N_0 = 100$, the power evolved by the booster was $\bar{W} = 0.5$ kW. The spectrometer resolution was $r = 3$ msec/m over a base line of 1000 m.

The IBR-30 Reactor. This reactor, started up on June 10, 1969, has been operating at an average power of $\bar{W} = 25$ kW since 1970, corresponding to a flux of $\bar{N} = 1.3 \cdot 10^{15}$ neutrons/sec into a solid angle of $4\pi$; the pulse period is $\tau = 1.5 \cdot 10^{-8}$ sec, the pulse length is $\theta = 70$ μsec, and the pulse power is $W_p = 100$ MW (at $f = 4$ $\text{sec}^{-1}$). The basic pulse repetition frequencies are $f = 100$ and 4 $\text{sec}^{-1}$, and the auxiliary frequencies are $f = 5$ and 10 $\text{sec}^{-1}$. At a power of $\bar{W} = 25$ kW, the average thermal-neutron flux from the moderator surface is $\bar{n}_{ther} = 5 \cdot 10^{10}$ neutrons/(sec · $\text{cm}^2$), while the flux at the pulse peak is $(n_{ther})_p = 10^{14}$ neutrons/(sec · $\text{cm}^2$). Within the moderator the pulsed neutron flux reaches $10^{15}$ neutrons/(sec · $\text{cm}^2$).

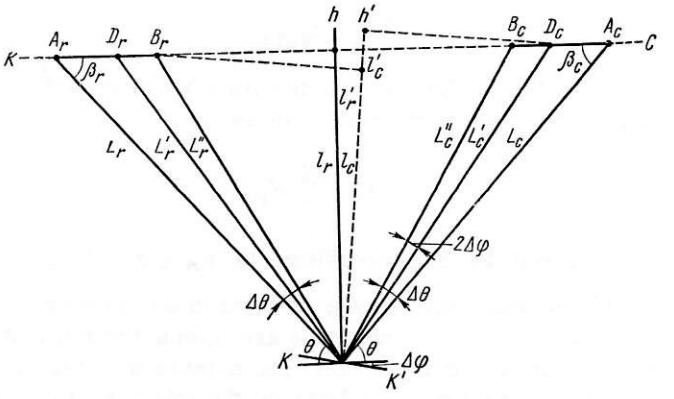


Fig. 39. Simplest example of time-of-flight focusing of neutrons during diffraction. R) Neutron source; C) neutron detector; K) crystal plane reflecting the neutrons. For the case of mirror reflection from plane K and for any path length $L'_r$ and the corresponding $L'_c$, we have $l_r = l_c = \text{const}$. When the reflecting plane is reoriented to position K', $l_r$ decreases to $l'_r$, $l_c$ increases to $l'_c$, and their sum remains constant.

The resonance-neutron flux at 100 m from the reactor and at an average reactor power $\overline{W}$ (in kilowatts) per 1 cm$^2$ of detector per 1 sec is

$$N(E)=\frac{270}{E^{0,9}}\overline{W}\ \text{neutrons/(sec}\cdot\text{cm}^2\cdot\text{eV)},$$

where E is in electron volts.

The IBR-30 is also used in the isolated-pulse mode, with $f$ = 1/4.75 or 1/7.6 sec$^{-1}$; $\overline{W}\approx$ 10 kW; and $W_p = 1 \cdot 10^6$ kW. The injector, a 40-MeV linear electron accelerator put into operation on March 24, 1970, has the following parameters:

Pulsed current of $I_p$ = 200 mA,
$f$ = 100 sec$^{-1}$,
A plutonium carbide target,
$\theta$ = 3 msec at $N/N_0$ = 100,
Booster power of $\overline{W}$ = 3 kW.

The IBR-2 Reactor. Construction of the IBR-2 began at the end of 1969; the first experiments are planned for 1974. The following parameters are expected:

$\overline{W}$ = 4 MW,
$\theta$ = 90 $\mu$sec,
$\tau = 4.2 \cdot 10^{-8}$ sec,
Average neutron flux of $\overline{N} = 1.75 \cdot 10^{17}$ neutrons/sec into a solid angle of $4\pi$,
Average thermal-neutron flux from moderator surface of $\overline{n}_{ther} = 5.8 \cdot 10^{12}$ neutrons/(sec · cm$^2$),
Pulsed thermal-neutron flux of $(n_{ther})_p = 10^{16}$ neutrons/(sec · cm$^2$) from the moderator surface and $(n_{ther})_p = 10^{17}$ neutrons/(sec · cm$^2$) inside it.

## APPENDIX 3

### Time-of-Flight Focusing in Diffraction

As was shown in the main text, the neutron time of flight as the neutrons are reflected from the crystal planes satisfies

$$t=\frac{l_r+l_c}{v_z} \qquad (1)$$

where $l_r$ and $l_c$ are the projections of the path lengths $L_r$ and $L_c$ from the source to the crystal and from the crystal to the detector on the normal to the reflecting planes. From the Bragg conditions we find that $v_z$ (the projection of the neutron velocity on this normal) should be

$$v_z d = n\left(\frac{h}{2m}\right), \tag{2}$$

where d is the distance between crystal planes, $h = 6.62 \cdot 10^{-27}$ is the Planck constant, and $m = 1.67 \cdot 10^{-24}$ is the mass of the neutron. We thus find $2m/h = 505$, and

$$t = \frac{l_r + l_c}{n}\, 505d \tag{3}$$

where all quantities are expressed in terms of centimeters and seconds.

From Eq. (3) we see that the neutron velocity and angle of incidence on the reflecting plane do not appear in the diffraction equation, but the angle of incidence obviously must be equal to the angle of reflection.

Accordingly, it is not difficult to see that time-of-flight focusing can be achieved during diffraction. Let us consider the extremely simple example illustrated in Fig. 39. Here we have $L_r = L_c$; the plane of the neutron source is parallel to the detector plane; and both are perpendicular to the normal h to the reflecting plane K of the crystal. We assume the crystal dimensions to be negligibly small. We see from this figure that a neutron emitted from some point $D_r$ of the surface of the neutron source and incident on the crystal, i.e., which moves in the direction $L'_r$ after reflection (the angle of incidence is equal to the angle of reflection), arrives along $L'_c$ at point $D_c$. Since the neutron-source and detector planes are perpendicular to h, the projections $l_r$ and $l_c$ of vectors $L'_c$ and $L'_r$ do not depend on the positions of $D_r$ and $D_c$. The time of flight is thus constant for all points $D_r$ during neutron diffraction.

Here we have not used the requirement that the source and detector planes be equidistant from the crystal. However, this requirement must be satisfied in order that the time-of-flight focusing occur, not only for plane K, but also plane K', which forms a small angle $\Delta\varphi$ with K (the normal to K' is h'). Then a neutron emitted from, e.g., point $B_r$ along the direction $L''_r$ does not pass along direction $L'_c$ after reflection, but deviates from it by an angle $2\Delta\varphi$, and passes along $L'_c$ to the point $D_c$. The projection of $L''_r$ on the normal h' is smaller than $l_r$, and the projection of $L'_c$ on h' is larger by an equal amount. Accordingly, the sum of the projections satisfies $l'_r + l'_c = l_r + l_c$, so the time of flight in (3) remains constant. However, the effective areas of the detector and source are smaller; i.e., the diffraction intensity is lower. It vanishes when the slope of the reflecting plane increases to $\Delta\theta = 0.5\Delta\theta$ (Fig. 39).

It is not difficult to see that this case is a particular case of time-of-flight focusing. In general, we can choose arbitrary values for $L_r$ and $L_c$. In this case, however, the source and detector planes have to be arranged at some definite angles $\beta_r$ and $\beta_c$ with respect to $L_r$ and $L_c$ (these angles are shown in Fig. 39), instead of being parallel. According to Holas, these angles are found from

$$L_r \operatorname{ctg}\beta_r - \frac{l_r + L_c}{2}\operatorname{ctg}\theta = 0; \tag{4}$$

$$L_c \operatorname{ctg}\beta_c - \frac{L_r + L_c}{2}\operatorname{ctg}\theta = 0. \tag{5}$$

Here $\theta$ is the angle between $L_r$ or $L_c$ and the reflecting plane of crystal (Fig. 41). In the particular case in which we have $L_r = L_c$, we evidently have $\beta_r = \beta_c = \theta$, as shown in Fig. 39.

We have assumed here that the crystal has a very small area. Holas showed that even this restriction can be relaxed.

## LITERATURE CITED


1. G. E. Blokhin, D. I. Blokhintsev, et al., At. Énerg., 10, 437 (1961).
2. I. M. Frank, Preprint R-6784, JINR (1961).
3. V. D. Anan'ev et al., Preprint 2372, JINR (1965).

4. V. D. Anan'ev et al., Preprint 13-5495, JINR (1969).
5. I. I. Bondarenko and Yu. Ya. Stavisskii, At. Énerg., 7, 417 (1959).
6. V. D. Anan'ev et al., Preprint 13-4392, JINR (1969).
7. I. Visi et al., Nuclear Electronics, I, IAEA, Vienna (1962), p. 27.
8. Wang Nai-yen, I. Visi, et al., Preprint R-1313, JINR (1963); Zh. Éksp. Teor. Fiz., 45, 1743 (1963).
9. L. B. Pikel'ner, et al., Pribory i Tekh. Éksperim., No. 2, 48 (1963).
10. Wang Shih-ti and Yu. V. Ryabov, Preprint 1685, JINR (1964).
11. N. W. Glass et al., Proceedings of the Second Conference on Neutron Cross Sections and Technology, Washington (1968), p. 573.
12. J. L. Rosen, et al., Phys. Rev., 118, 687 (1960).
13. M. Asghar, C. M. Chaffey, and M. C. Moxon, Nucl. Phys., 85, 305 (1966).
14. H. Malecki, L. B. Pikel'ner, I. M. Salamatin, and É. I. Sharapov, Report to the Soviet-French Seminar on Nuclear Data, Dubna, June 22-24, 1970); Preprint R3-5609, JINR (1971).
15. H. Malecki, L. B. Pikel'ner, I. M. Salamatin, and E. I. Sharapov, Preprint R3-4929, JINR (1970).
16. V. I. Furman and A. B. Popov, Preprint R4-3925 (1968).
17. Yu. V. Ryabov, Wang yung-ch'ang, E. Dermendzhev, and Chang P'o-shu, Preprint R-2713, JINR (1966).
18. I. M. Frank, Proceedings of the Working Conference on Interactions of Neutrons with Nuclei, June 9-12, 1964; Preprint 1845, JINR (1964), p. 133.
19. Yu. V. Ryabov, Physics and Chemistry of Fission, IAEA, Vienna (1969), p. 486.
20. S. Weinstein and R. C. Block, Phys. Rev. Lett., 22, 195 (1969).
21. E. Dermendzhev and Ts. Panteleev, Report R3-5081, JINR (1970).
22. Yu. V. Ryabov, So Tong-hsik, N. Chikov, and M. A. Kurov, Report R3-5113, JINR (1970).
23. K. A. Gavrilov, K. K. Koshaeva, S. N. Kraitor, and L. B. Pikel'ner, Preprint R3-4449, JINR (1969); At. Énerg., 28, 362 (1970).
24. D. Paya et al., Nuclear Data for Reactors, 11, IAEA, Vienna, p. 128.
25. L. B. Pikel'ner, in: Problems of Elementary-Particle and Nuclear Physics [in Russian], Vol. 2, No. 4, Atomizdat, Moscow (1971).
26. H. Malecki, L. B. Pikel'ner, I. M. Salamatin, and É. I. Sharapov, Preprint R3-3456, JINR (1967); Yad. Fiz., 9, 1119 (1969); Preprint R3-4152, JINR (1968); Yad. Fiz., 11, 111 (1970).
27. É. N. Karzhavina, Nguyen Nguyen Phong, and A. B. Popov, Preprint R3-3882, JINR (1968); Yad. Fiz., 9, 897 (1969).
28. Yu. V. Taran and F. L. Shapiro, Zh. Éksp. Teor. Fiz., 44, 2185 (1963).
29. V. P. Alfimenkov et al., Yad. Fiz., 3, 55 (1966).
30. V. P. Alfimenkov et al., Phys. Lett., 24, 151 (1967); S. I. Ivanenko, V. I. Lushchikov, Yu. V. Taran, and F. L. Shapiro, Yad. Fiz., 10, 47 (1969).
31. J. Urbanec et al., Czechosl. J. Phys., B19, 899 (1969).
32. J. Urbanec et al., Czechosl. J. Phys., 19, 248 (1969).
33. J. Kvitek and Yu. P. Popov, Phys. Lett., 22, 186 (1966); J. Kvitek and Yu. P. Popov, ZhÉTF Pis. Red., 4, 365 (1967).
34. V. G. Solov'ev, Preprint E4-5135, JINR (1970).
35. D. J. Hughes et al. Phys. Rev., 119, 872 (1960); V. V. Golikov et al., Inelastic Scattering of Neutrons in Solids and Liquids, Vol. 2, Vienna (1965), p. 201.
36. T. A. Machekina, Z. I. Ogzheval'skii, and F. L. Shapiro, Proceedings of the Working Conference on the Physics of Slow Neutrons, Dubna (1962), p. 1956.
37. A. Baiiorek, T. A. Machekina, K. Parlin'ski, and F. L. Shapiro, Preprint R-1899, JINR (1964).
38. V. V. Golikov and Zh. A. Kozlov, Preprint R14-4355, JINR (1969).
39. L. A. Bulavin et al., Preprint R14-3824, JINR (1968).
40. L. A. Bulavin et al., Preprint R14-4829, JINR (1969); L. P. Bulavin, Yu. M. Ostanevich, and A. P. Simkina, Preprint R14-4830, JINR (1969).
41. V. G. Liforov et al., Preprint 129, FTI (1968).
42. B. Buras, Research Applications of Nuclear Pulsed Systems, Proceedings of a Panel, Dubna, July 18-22, 1966; Vienna, 1967; B. Buras and J. Leciejewicj, Phys. Stat. Sol., 4, 349 (1964).
43. V. V. Nitts, I. Sosnovska, E. Sosnovska, and F. L. Shapiro, Preprint R-2081, JINR (1965); B. Buras et al., Proceedings of the 3rd UN Conference on the Peaceful Uses of Atomic Energy, Vol. 7, Geneva (1964), p. 441.
44. A. Holas, Nukleonika, 13, 871 (1968); A. Holas et al., Nucl. Instrum. Methods, 69, 1731 (1969).

45. V. V. Nitts, Z. G. Papulova, I. Sosnovaka, and E. Sosnovska, Fiz. Tverd. Tela, 6, 1369 (1964); V. V. Nitts, I. Sosnovska, E. Sosnovska, and F. L. Shapiro, Preprint 2081, JINR (1965).
46. P. S. Antsupov et al., Preprint R14-4548, JINR (1969).
47. Yu. A. Aleksandrov, in: Problems of Elementary-Particle Nuclear Physics [in Russian], Vol. I, No. 2 (1971), p. 546; Preprint R3-4783, JINR (1969).
48. Yu. A. Aleksandrov and G. S. Samosvat, Report R3-4353, JINR (1969); Yad. Fiz., 11, 1152 (1970).
49. V. I. Lushchikov et al., ZhÉTF Pis. Red., 9, 40 (1969); Preprint R3-4127, JINR (1968).
50. Ya. B. Zel'dovich, Zh. Éksp. Teor. Fiz., 36, 1952 (1959).
51. L. V. Groshev et al., Preprint R3-5392, JINR (1970).